



Memo version 2.1

# BESIII Analysis Memo

BAM-697

January 5, 2024

## First measurement of $\Lambda_c^+ \rightarrow n K_S^0 \pi^+ \pi^0$ at BESIII

Yunlong Xiao<sup>a</sup>, Linxuan Zhu<sup>b</sup>, Liang Yan<sup>a</sup>, Xiao-Rui Lyu<sup>b</sup>, and Yangheng Zheng<sup>b</sup>

<sup>a</sup>*Fudan University, People's Republic of China*

<sup>b</sup>*University of Chinese Academy of Sciences, People's Republic of China*

## Referee Committee

Cong Geng (Chair)<sup>1</sup>, Jiajia Qin<sup>2</sup>, Yinghao Wang<sup>3</sup>

<sup>1</sup>*Sun Yat-Sen University*

<sup>2</sup>*University of South China*

<sup>3</sup>*Lanzhou University*

## Pubcomm Editors

Chunhua Li<sup>g</sup>, Roy Briere<sup>h</sup>

<sup>g</sup>*Liaoning Normal University*

<sup>h</sup>*Carnegie Mellon University*

HN : <http://hnbes3.ihep.ac.cn/HyperNews/get/paper697.html>

## Abstract

Using data of  $4.5 \text{ fb}^{-1}$   $\Lambda_c^+ \bar{\Lambda}_c^-$  pairs taken with the Beijing Spectrometer (BESIII) at the Beijing Electron-Positron Collider (BEPCII), the Cabibbo-Favored process  $\Lambda_c^+ \rightarrow n K_S^0 \pi^+ \pi^0$  has been measured exclusively. The branching fraction of  $\Lambda_c^+ \rightarrow n K_S^0 \pi^+ \pi^0$  is measured to be  $(0.85 \pm 0.13 \pm 0.03) \times 10^{-2}$  for the first time.

## 20 **Contents**

21	<b>1 ChangeLog</b>	3
22	<b>2 Introduction</b>	4
23	<b>3 The BEPCII and BESIII detector</b>	6
24	<b>4 Data and Monte Carlo</b>	7
25	4.1 Data sets . . . . .	7
26	4.2 Monte Carlo Simulation and Method . . . . .	7
27	4.3 Decay chain . . . . .	8
28	<b>5 Analysis strategy</b>	9
29	<b>6 Event Selections of ST</b>	11
30	<b>7 Event Selections of DT for <math>\Lambda_c^+ \rightarrow n K_S^0 \pi^+ \pi^0</math></b>	13
31	7.1 Track Level Selection . . . . .	13
32	7.2 $K_S^0$ reconstruction . . . . .	13
33	7.3 Good charged track for the bachelor $\pi^+$ . . . . .	13
34	7.4 $\pi^0$ reconstruction . . . . .	14
35	<b>8 Study of backgrounds</b>	16
36	8.1 Background analysis . . . . .	16
37	<b>9 Branching fraction measurement</b>	19
38	9.1 Summary of event selection criteria and cut flow . . . . .	19
39	9.2 DT efficiency . . . . .	19
40	9.3 Branching fraction . . . . .	20
41	<b>10 Systematic uncertainties of branching fraction measurement</b>	25
42	10.1 Tracking and PID . . . . .	25
43	10.2 $\pi^0$ reconstruction . . . . .	25
44	10.3 $K_S^0$ reconstruction . . . . .	26
45	10.4 Branching fraction . . . . .	26
46	10.5 Fitting model in the ST side . . . . .	26
47	10.6 MC statistics . . . . .	26

48	10.7 Fitting model . . . . .	26
49	10.8 Veto peaking background . . . . .	29
50	10.9 MC Model . . . . .	31
51	<b>11 Summary</b>	<b>34</b>
52	<b>A Appendices</b>	<b>37</b>
53	A.1 Other comparison with PHSP MC in the signal region . . . . .	43
54	A.2 Other comparison with Weight MC in the signal region . . . . .	45
55	A.3 Selection efficiency before vetoing peaking backgrounds . . . . .	46
56	A.4 IO check for branching fraction . . . . .	47
57	A.5 smearing parameters for the control sample $\Lambda_c^+ \rightarrow \Lambda(n\pi^0)\pi^+$ . . . . .	48
58	A.6 Background analysis . . . . .	48
59	<b>B Check for fitting method</b>	<b>49</b>
60	<b>C Shape convolved by 2D Gaussian with correlation coefficients</b>	<b>50</b>
61	<b>D 2D fit to the distributions of the invariant mass of <math>n</math> and <math>\pi^+\pi^-</math></b>	<b>51</b>

## 62 **1 ChangeLog**

### 63 From Memo V1.6 to Memo V1.7:

64 The main change is that:

65 According to the suggestions from referee (JiaJia Qing), the systematic uncertainties of  $K_S^0$ ,  $\pi^+$ , and  
66  $\pi^0$  have optimized using control samples.

67 According to the suggestions from referee (Yinghao Wang), some theoretical references of  $\Lambda_c^+$   
68 branching fraction measurement have been added and compared with our measurement in the summary.

69

### 70 From Memo V1.7 to Memo V1.8:

71 The main change is that:

72 According to the suggestions from referee (Cong Geng), the distributions of  $M(\pi^+\pi^-)$ ,  $dL/d\sigma$ , and  
73 other charged tracks (excluding  $\pi^+\pi^-$  from  $K_S^0$ ) have been added in the updated version.

74 The cutflow of signal MC has been added in the updated version.

75

### 76 From Memo V1.8 to Memo V1.9:

77 The main change is that:

78 According to the suggestions from referee (JiaJia Qing), the ChangeLog has been added in the preface  
79 and the change of branching fraction has been explained.

## 80 2 Introduction

81        The lightest charmed baryon  $\Lambda_c^+$  was first observed in  $e^+e^-$  annihilation at the Mark II experiment [1],  
 82   studying of its hadronic decays can provide important information to understand both the strong and the  
 83   weak interactions. Recently, many  $\Lambda_c^+$  decay modes (70% of the branching fraction for  $\Lambda_c^+$  [2]) have been  
 84   measured by BESIII, BELLE and etc., which means that about 30% decay modes still needs exploiting,  
 85   clean  $\Lambda_c^+$  pairs are produced via electron-positron annihilation, which provides a unique environment to  
 86   accurately measure the production and decay of  $\Lambda_c^+$ , and then provides an opportunity to further study  
 87   unknown decay modes.

88        On the one hand, the total branching fraction of  $\Lambda_c^+$  involving a neutron is measured to be  $(33.5 \pm$   
 89    $0.7 \pm 1.2)\%$  [3]. Therefore, the measurement of branching fraction of  $\Lambda_c^+$  decaying to neutron is also a  
 90   very interesting topic in high energy physics community. On the other hand, the branching fractions of  
 91   Cabibbo-favored decays  $\Lambda_c^+ \rightarrow pK^-\pi^+\pi^0$  [4],  $\Lambda_c^+ \rightarrow nK^-\pi^+\pi^+$  [5] and  $\Lambda_c^+ \rightarrow pK_S^0\pi^+\pi^-$  [4] have been  
 92   measured at BESIII. However, the isospin symmetry process  $\Lambda_c^+ \rightarrow nK_S^0\pi^+\pi^0$  has not been observed yet,  
 93   as illustrated in Tab. 1. Here, no theoretical calculations for the branching fraction of  $\Lambda_c^+ \rightarrow nK_S^0\pi^+\pi^0$   
 94   are reported. Therefore, our measurement can provide important input for theoretical research.

95        The decay amplitude of the charmed baryon generally consists of factorizable and non-factorizable  
 96   contributions. It is known that the non-factorizable contribution is negligible comparing to the fac-  
 97   torizable contribution in describing the non-leptonic weak decays of charmed mesons. However, the  
 98   truth is quite opposite for charmed baryon decays.  $\Lambda_c^+ \rightarrow nK_S^0\pi^+\pi^0$  proceeds through internal W-  
 99   emission, external W-emission and W-exchange processes, as shown in Fig 1. Therefore, the dynamics  
 100   of  $\Lambda_c^+ \rightarrow nK_S^0\pi^+\pi^0$  includes both factorizable and non-factorizable contributions. Charge conjugation is  
 101   always implied throughout the memo, except explicitly mentioned.

Tab. 1: The branching fraction of isospin symmetry process

Decay mode	Branching fraction( $\times 10^{-2}$ )
$\Lambda_c^+ \rightarrow pK^-\pi^+\pi^0$	$4.46 \pm 0.30$ [4]
$\Lambda_c^+ \rightarrow nK^-\pi^+\pi^+$	$1.87 \pm 0.12$ [5]
$\Lambda_c^+ \rightarrow pK_S^0\pi^+\pi^-$	$1.60 \pm 0.12$ [4]
$\Lambda_c^+ \rightarrow nK_S^0\pi^+\pi^0$	–

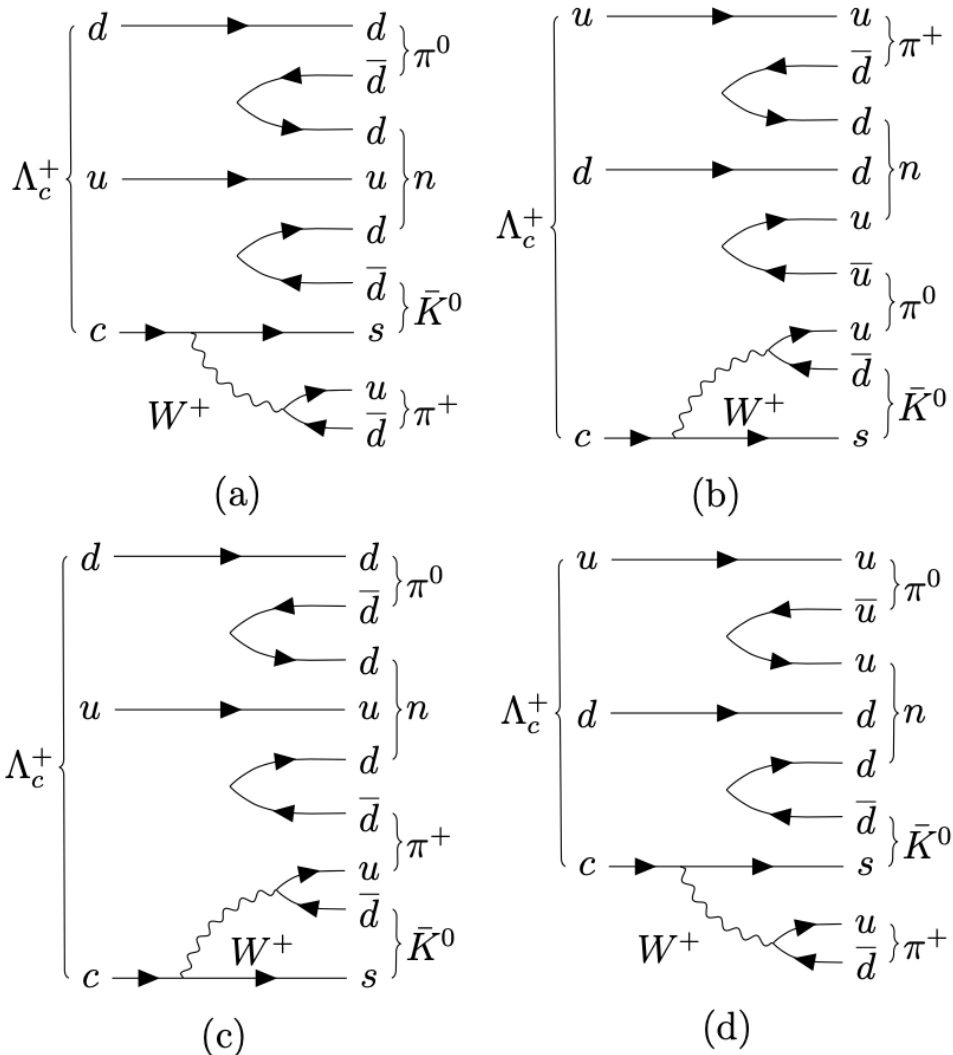


Fig. 1: Feynman diagrams for  $\Lambda_c^+ \rightarrow n K_S^0 \pi^+ \pi^0$ , (a)(d)External W-emission and W-exchange diagram and (b)(c)Internal W-emission and W-exchange diagram.

### 102    3 The BEPCII and BESIII detector

103       The BESIII detector [6] records symmetric  $e^+e^-$  collisions provided by the BEPCII storage ring [7],  
104      which operates with a peak luminosity of  $1 \times 10^{33} \text{ cm}^{-2}\text{s}^{-1}$  in the center of mass energy range from  
105      2.0 to 4.9 GeV. BESIII has collected large data samples in this energy region [8]. The cylindrical core  
106      of the BESIII detector covers 93% of the full solid angle and consists of a helium-based multilayer  
107      drift chamber (MDC), a plastic scintillator time-of-flight system (TOF), and a CsI(Tl) electromagnetic  
108      calorimeter (EMC), which are all enclosed in a superconducting solenoidal magnet providing a 1.0 T (0.9  
109      T in 2012) magnetic field. The solenoid is supported by an octagonal flux-return yoke with resistive plate  
110      counter muon identification modules interleaved with steel. The charged-particle momentum resolution  
111      at 1 GeV/c is 0.5%, and the dE/dx resolution is 6% for electrons from Bhabha scattering. The EMC  
112      measures photon energies with a resolution of 2.5% (5%) at 1 GeV in the barrel (end cap) region. The  
113      time resolution in the TOF barrel region is 68 ps, while that in the end cap region is 110 ps. The end cap  
114      TOF system was upgraded in 2015 using multi-gap resistive plate chamber technology, providing a time  
115      resolution of 60 ps [9].

## 116 4 Data and Monte Carlo

### 117 4.1 Data sets

118 The data sample of  $\Lambda_c^+$  events has been collected with the  $4.5 \text{ fb}^{-1}$   $e^+e^-$  data in the energy region  
 119 between 4.6 GeV and 4.7 GeV by the BESIII detector at the BEPCII collider. The energy points are  
 120 above the  $\Lambda_c^+$  pair production threshold, and the details of each energy points are presented in Tab 2.

Tab. 2: Energy points collected beyond the  $\Lambda_c^+$  pair production threshold at BESIII

Nominal Energy Points (GeV)	$E_{\text{cms}}$ (MeV)	Luminosity ( $\text{pb}^{-1}$ )	Boss Version
4.600	$4599.94 \pm 0.29$	$566.93 \pm 0.11$	7.0.6
4.612	$4611.86 \pm 0.34$	$103.83 \pm 0.55$	7.0.6
4.628	$4628.00 \pm 0.32$	$521.52 \pm 2.76$	7.0.6
4.641	$4640.91 \pm 0.38$	$552.41 \pm 2.93$	7.0.6
4.661	$4661.24 \pm 0.30$	$529.63 \pm 2.81$	7.0.6
4.682	$4661.92 \pm 0.30$	$1659.31 \pm 8.85$	7.0.6
4.699	$4698.82 \pm 0.40$	$536.45 \pm 2.84$	7.0.6

### 121 4.2 Monte Carlo Simulation and Method

122 Simulated samples produced with the GEANT4-based [10] Monte Carlo (MC) package which in-  
 123 cludes the geometric description of the BESIII detector and the detector response, are used to determine  
 124 the detection efficiency and to estimate the backgrounds. The  $\psi(3686)$  resonance is simulated with the  
 125 KKMC generator [11], which is an event generator based on precise predictions of the Electroweak  
 126 Standard Model for the process. The beam energy spread and initial state radiation (ISR) are taken into  
 127 account in the simulation. The software framework used for the data analysis is BOSS(BESIII Offline  
 128 Software System), which is developed from Gaudi. This work is under BOSS version 7.0.6. About  
 129 inclusive MC events of forty times larger than the real data sets and hadron MC events of ten times  
 130 larger than the real data sets are used to investigate possible backgrounds. The known decay modes are  
 131 modelled with EVTGEN [12] using branching fractions taken from the Particle Data Group [17], and the  
 132 remaining unknown charmonium decays are modelled with LUNDCHARM [13]. Final state radiation  
 133 (FSR) from charged final state particles is incorporated using the PHOTOS package.

134 We generate three types of Monte Carlo events: Cocktail MC events [14] are used to understand the  
 135 background components and also to obtain the detection efficiency. The Cocktail MC sample consists  
 136 of decays of ISR-produced low  $\psi$  states, charm meson ( $D$  and  $D_s$ ) productions,  $\Lambda_c^+\bar{\Lambda}_c^-$  pair events and  
 137 QED processes and continuum processes. The detailed information of the MC samples used in this  
 138 analysis are shown in Tab. 3, in which the cross sections for various of the processes are summarized. In  
 139 MC generation, the generated inclusive samples are 40 times larger than data. For other processes, the

<sup>140</sup> generated hadron samples are 10 times larger than data.

<sup>141</sup> For the signal processes: ST signal shape events, the  $\bar{\Lambda}_c^-$  decays into one of the 11 tag modes while  
<sup>142</sup> the other  $\Lambda_c^+$  decays into invisible mode exclusively. The ST signal shape MC can be used as signal  
<sup>143</sup> shape both for fitting data and Cocktail MC to extract ST yields and efficiencies. DT signal MC events,  
<sup>144</sup> the  $\bar{\Lambda}_c^-$  decay into one of the 11 tag modes while the other  $\Lambda_c^+$  decays into signal channel. We use DT  
<sup>145</sup> signal MC sample to obtain the DT efficiencies.

Tab. 3: Energy points collected beyond the  $\Lambda_c^+$  pair production threshold at BESIII

Energy (GeV)	$\sigma_{\Lambda_c^+\bar{\Lambda}_c^-}$ (pb)	$\sigma_{\text{hadron}}$ (nb)	$\sigma_{\text{bhabha}}$ (nb)	$\sigma_{\mu^+\mu^-}$ (nb)	$\sigma_{\tau^+\tau^-}$ (nb)	$\sigma_{\text{two photon}}$ (nb)
4.600	162.34	17.9325	351.249	4.34393	3.40368	2.05389
4.612	162.69	17.8398	348.652	4.32145	3.39772	2.06232
4.628	170.39	17.7228	346.682	4.2954	3.38914	2.07491
4.641	174.29	17.6402	344.662	4.27001	3.38268	2.08448
4.661	170.12	17.5143	341.629	4.23729	3.37149	2.09552
4.682	163.19	17.3765	338.545	4.19507	3.36007	2.11523
4.699	156.63	17.2786	336.480	4.16924	3.35188	2.12758

### <sup>146</sup> 4.3 Decay chain

<sup>147</sup> In this analysis, the concerned decay channel is  $\Lambda_c^+ \rightarrow nK_S^0\pi^+\pi^0$ , where  $K_S^0$  is reconstructed from  
<sup>148</sup>  $\pi^+\pi^-$  and  $\pi^0$  is reconstructed from  $\gamma\gamma$ . Here, PHSP model is used to produce signal MC.

## 149 5 Analysis strategy

150 Using a technique firstly introduced by the MARK III Collaboration [15], the  $\Lambda_c^+$  is reconstructed  
 151 by some tag modes, and double tag (DT) events decay to recoiling against the ST particle. For decay  
 152 channel, we combine the 11 ST ( $\bar{p}K_S^0$ ,  $\bar{p}K^+\pi^-$ ,  $\bar{p}K_S^0\pi^0$ ,  $\bar{p}K_S^0\pi^-\pi^+$ ,  $\bar{p}K^+\pi^-\pi^0$ ,  $\bar{\Lambda}\pi^-$ ,  $\bar{\Lambda}\pi^-\pi^0$ ,  
 153  $\bar{\Sigma}^0\pi^-$ ,  $\bar{\Sigma}^-\pi^0$ , and  $\bar{\Sigma}^-\pi^-\pi^+$ ) decay modes to obtain the branching fraction. Here,  $\Lambda_c^+ \rightarrow p\pi^+\pi^-$  channel is  
 154 removed because this background level is very high. For ST, we employ the  $\Delta E$  and the beam constrained  
 155 mass  $M_{BC}$  to get the tag yields. The  $\Delta E$  and  $M_{BC}$  is defined as:

$$\Delta E = E_{\text{tag}} - E_{\text{beam}} \quad (1)$$

$$M_{BC} = \sqrt{E_{\text{beam}}^2/c^4 - |p_{\Lambda_c^+}|^2/c^2}, \quad (2)$$

156 where  $E_{\text{beam}}$  is the beam energy,  $E_{\text{tag}}$  is the reconstructive energy of  $\Lambda_c^+$ , and  $|p_{\Lambda_c^+}|$  is the momentum of  
 157 the  $\Lambda_c^+$  candidate.

158 For each decay channel, the relative yields of ST events to DT events can then be obtained, with  
 159 correction of their relative tagging efficiencies estimated in MC simulations. Therefore, it will provide  
 160 a clean and model-independent BF measurement without knowing the total number of  $\Lambda_c^+$  events. If CP  
 161 violation is negligible, the BF of  $\Lambda_c^+$  decay to tag mode  $i^+$ ,  $B_i$  and  $\bar{\Lambda}_c^-$  decay to mode  $i^-$ ,  $B_{i^-}$ , are equal.  
 162 Therefore, we denote  $B_{i^+} = B_{i^-} = B_i$ . The observed yields of reconstructed  $\Lambda_c^+ \rightarrow i^+$  and  $\bar{\Lambda}_c^- \rightarrow i^-$  ST  
 163 events  $N_i^{\text{ST}}$ , can be written as:

$$N_i^{\text{ST}} = 2 \times N_{\Lambda_c^+ \bar{\Lambda}_c^-} \times B_i \times \varepsilon_{i,s}^{\text{ST}}, \quad (3)$$

164 where  $N_{\Lambda_c^+ \bar{\Lambda}_c^-}$  is the total number of  $\Lambda_c^+ \bar{\Lambda}_c^-$  pairs produced and  $\varepsilon_{i,s}^{\text{ST}}$  is the efficiency for detecting a ST  
 165 mode  $i$ . The DT yields  $N_{i,s}^{\text{DT}}$  which combined  $\bar{\Lambda}_c^- \rightarrow i^-$ ,  $\Lambda_c^+ \rightarrow s$  and  $\Lambda_c^+ \rightarrow i$ ,  $\bar{\Lambda}_c^- \rightarrow s$  events will be

$$N_{i,s}^{\text{DT}} = 2 \times N_{\Lambda_c^+ \bar{\Lambda}_c^-} \times B_i \times B_s \times B_{\text{sub}} \times \varepsilon_{i,s}^{\text{DT}}, \quad (4)$$

166 where  $\varepsilon_{i,s}^{\text{DT}}$  is the efficiency for detecting DT modes  $i$  and  $s$ , and  $B_{\text{sub}}$  is equal to be  $B(K_S^0 \rightarrow \pi^+\pi^-) \times$   
 167  $B(\pi^0 \rightarrow \gamma\gamma)$ . If we take the ratio of Eq. 4 to Eq. 3, we have total yields of DT mode  $s$  over the 11 ST  
 168 mode  $i$  at  $\sqrt{s} = \alpha$ , where  $\alpha = 4.600$  GeV, 4.612 GeV, 4.628 GeV, 4.641 GeV, 4.661 GeV, 4.682 GeV,  
 169 4.699 GeV, which is formulated as:

$$N_{-,s}^{\alpha,\text{DT}} = \sum_i N_{i,s}^{\alpha,\text{DT}} = \sum_i \left( \frac{N_i^{\alpha,\text{ST}}}{\varepsilon_i^{\alpha,\text{ST}}} \times B_s \times B_{\text{sub}} \times \varepsilon_{i,s}^{\text{DT}} \right) = B_s \times B_{\text{sub}} \times \sum_i \left( \frac{N_i^{\alpha,\text{ST}}}{\varepsilon_i^{\alpha,\text{ST}}} \times \varepsilon_{i,s}^{\text{DT}} \right) \quad (5)$$

<sup>170</sup> Eq. 5 provides an absolute measurement of the BF  $B_s$ .

$$B_s = \frac{N_{-,s}^{\alpha,DT}}{B_{sub} \times \sum_i (\frac{N_i^{\alpha,ST}}{\varepsilon_i^{\alpha,ST}} \times \varepsilon_{i,s}^{DT})} \quad (6)$$

<sup>171</sup> For the Eq. 6, the  $i$  is the label of the  $i$  tag mode. In this analysis, we use the data taken among  $\sqrt{s} =$   
<sup>172</sup> 4.600GeV to 4.699 GeV to calculate the BF  $B_{final}$  signal. Thus, we obtain

$$B_{final\ signal} = \frac{\sum_{\alpha} N_{-,s}^{\alpha,DT}}{B_{sub} \times \sum_{\alpha} \sum_i (\frac{N_i^{\alpha,ST}}{\varepsilon_i^{\alpha,ST}} \times \varepsilon_{i,s}^{DT})} = \frac{N_{-,s}^{DT}}{B_{sub} \times \sum_{\alpha} \sum_i (\frac{N_i^{\alpha,ST}}{\varepsilon_i^{\alpha,ST}} \times \varepsilon_{i,s}^{DT})}, \quad (7)$$

<sup>173</sup> where  $\alpha$  is the label of the energy point  $\alpha$ . In this way, most of systematic uncertainties from tag sides  
<sup>174</sup> are canceled.

<sup>175</sup> For DT, the recoiling information of the signal  $K_S^0 \pi^+ \pi^0$  is used to extract the yield of  $\Lambda_c^+ \rightarrow n K_S^0 \pi^+ \pi^0$   
<sup>176</sup> and obtain the result of branching fraction based on Eq.7.

## 177 6 Event Selections of ST

178     The  $\bar{\Lambda}_c^-$  is reconstructed and  $M_{BC}$  is determined by combining the 11 ST channels ( $\bar{p}K_S^0$ ,  $\bar{p}K^+\pi^-$ ,  
 179      $\bar{p}K_S^0\pi^0$ ,  $\bar{p}K_S^0\pi^-\pi^+$ ,  $\bar{p}K^+\pi^-\pi^0$ ,  $\bar{\Lambda}\pi^-$ ,  $\bar{\Lambda}\pi^-\pi^0$ ,  $\bar{\Lambda}\pi^-\pi^+\pi^-$ ,  $\bar{\Sigma}^0\pi^-$ ,  $\bar{\Sigma}^-\pi^0$ , and  
 180      $\bar{\Sigma}^-\pi^-\pi^+$ ). The ST selection criteria are the same as BAM-563 [5] and are not repeated herein.

181     For the ST analysis, if there is more than one candidate in a decay mode, we select the best one with  
 182     minimal  $|\Delta E|$ , whcih are shown in Figs. 17, 18, 19, 20, 21, and 22.

183     We obtain ST yields in data and MC events with unbinned maximum likelihood fits to the  $M_{BC}$  dis-  
 184     tributions. Each fit includes a signal shape function for signals and an ARGUS function for backgrounds.  
 185     The signal shape is obtained from convolution of the signal MC shape with a Gaussian function, while  
 186     the signal MC shape is extract from ST signal shape MC. The background ARGUS parameters truncation  
 187     m is fixed to the value of beam energy. The  $M_{BC}$  signal region and  $M_{BC}$  side-band region are defined  
 188     as the mass window (2.280, 2.296)  $\text{GeV}/c^2$  and mass window (2.250, 2.270)  $\text{GeV}/c^2$ , which contribute  
 189     two data sets to study signal and background contributions.

190     Tab. 4 and Tab. 5 gives the ST yields in data and the ST efficiencies, which correspond to  $N_i^{ST}$  and  
 191      $\epsilon_{i,s}^{ST}$  in Eq. 3, respectively.

Tab. 4: ST yields which combined charge conjugation modes from  $\sqrt{s} = 4.600 \text{ GeV}$  to  $4.699 \text{ GeV}$ .

Modes	4.600 GeV	4.612 GeV	4.628 GeV	4.641 GeV	4.661 GeV	4.682 GeV	4.699 GeV
$pK_S^0$	$1243 \pm 35$	$226 \pm 15$	$994 \pm 33$	$1048 \pm 34$	$1044 \pm 33$	$3141 \pm 57$	$889 \pm 30$
$pK^-\pi^+$	$6607 \pm 89$	$1094 \pm 37$	$5513 \pm 37$	$5842 \pm 83$	$5447 \pm 79$	$15919 \pm 134$	$4680 \pm 73$
$pK_S^0\pi^+$	$587 \pm 33$	$119 \pm 16$	$569 \pm 33$	$552 \pm 33$	$527 \pm 32$	$1591 \pm 56$	$414 \pm 30$
$pK_S^0\pi^+\pi^-$	$594 \pm 33$	$100 \pm 15$	$475 \pm 30$	$484 \pm 30$	$487 \pm 21$	$1365 \pm 51$	$414 \pm 28$
$pK^-\pi^+\pi^0$	$1965 \pm 71$	$331 \pm 30$	$1453 \pm 75$	$1458 \pm 63$	$1460 \pm 63$	$4361 \pm 109$	$1172 \pm 62$
$\Lambda\pi^+$	$738 \pm 27$	$116 \pm 11$	$636 \pm 27$	$664 \pm 27$	$624 \pm 26$	$1916 \pm 45$	$495 \pm 23$
$\Lambda\pi^+\pi^0$	$1681 \pm 54$	$281 \pm 22$	$1342 \pm 50$	$1483 \pm 50$	$1338 \pm 46$	$3900 \pm 78$	$1145 \pm 43$
$\Lambda\pi^+\pi^-\pi^+$	$744 \pm 35$	$130 \pm 14$	$547 \pm 31$	$690 \pm 34$	$703 \pm 33$	$1847 \pm 55$	$569 \pm 31$
$\Sigma^0\pi^+$	$502 \pm 25$	$95 \pm 12$	$384 \pm 22$	$413 \pm 23$	$414 \pm 22$	$1267 \pm 38$	$334 \pm 20$
$\Sigma^+\pi^0$	$309 \pm 24$	$68 \pm 10$	$242 \pm 21$	$271 \pm 22$	$264 \pm 22$	$770 \pm 38$	$216 \pm 21$
$\Sigma^+\pi^+\pi^-$	$1146 \pm 47$	$204 \pm 21$	$922 \pm 19$	$995 \pm 46$	$949 \pm 44$	$2729 \pm 79$	$848 \pm 42$

Tab. 5: ST efficiencies(%) which combined charge conjugation modes from  $\sqrt{s} = 4.600$  GeV to 4.699 GeV.

Modes	4.600 GeV	4.612 GeV	4.628 GeV	4.641 GeV	4.661 GeV	4.682 GeV	4.699 GeV
$pK_S^0$	$54.6 \pm 0.2$	$50.8 \pm 0.6$	$48.9 \pm 0.2$	$47.9 \pm 0.2$	$46.4 \pm 0.2$	$45.2 \pm 0.1$	$44.1 \pm 0.2$
$pK^- \pi^+$	$49.9 \pm 0.1$	$47.8 \pm 0.2$	$46.1 \pm 0.1$	$45.3 \pm 0.1$	$44.3 \pm 0.1$	$42.8 \pm 0.1$	$41.9 \pm 0.1$
$pK_S^0 \pi^+$	$22.2 \pm 0.2$	$20.8 \pm 0.4$	$19.2 \pm 0.2$	$19.1 \pm 0.2$	$18.2 \pm 0.2$	$17.6 \pm 0.1$	$16.7 \pm 0.2$
$pK_S^0 \pi^+ \pi^-$	$22.8 \pm 0.2$	$20.4 \pm 0.4$	$19.2 \pm 0.2$	$19.3 \pm 0.2$	$18.3 \pm 0.2$	$18.7 \pm 0.1$	$17.4 \pm 0.2$
$pK^- \pi^+ \pi^0$	$19.4 \pm 0.1$	$18.1 \pm 0.2$	$16.8 \pm 0.1$	$16.2 \pm 0.1$	$15.7 \pm 0.1$	$15.4 \pm 0.0$	$14.9 \pm 0.1$
$\Lambda \pi^+$	$47.1 \pm 0.3$	$44.2 \pm 0.6$	$40.7 \pm 0.3$	$40.2 \pm 0.3$	$38.8 \pm 0.3$	$38.2 \pm 0.2$	$36.2 \pm 0.3$
$\Lambda \pi^+ \pi^0$	$20.8 \pm 0.1$	$18.4 \pm 0.2$	$17.6 \pm 0.1$	$17.5 \pm 0.1$	$16.9 \pm 0.1$	$16.1 \pm 0.1$	$15.7 \pm 0.1$
$\Lambda \pi^+ \pi^- \pi^+$	$15.1 \pm 0.1$	$12.7 \pm 0.3$	$12.7 \pm 0.1$	$13.2 \pm 0.1$	$12.7 \pm 0.1$	$12.5 \pm 0.1$	$13.0 \pm 0.1$
$\Sigma^0 \pi^+$	$28.4 \pm 0.2$	$24.8 \pm 0.5$	$25.3 \pm 0.2$	$24.2 \pm 0.2$	$24.0 \pm 0.2$	$23.2 \pm 0.1$	$21.9 \pm 0.2$
$\Sigma^+ \pi^0$	$22.8 \pm 0.3$	$21.0 \pm 0.6$	$21.5 \pm 0.3$	$22.3 \pm 0.3$	$20.5 \pm 0.3$	$19.6 \pm 0.1$	$18.3 \pm 0.3$
$\Sigma^+ \pi^+ \pi^-$	$24.5 \pm 0.1$	$23.8 \pm 0.3$	$21.9 \pm 0.1$	$21.6 \pm 0.1$	$20.9 \pm 0.1$	$20.0 \pm 0.1$	$19.9 \pm 0.1$

<sup>192</sup> Actually, the ST requirements are same as previous analyses and are standard criteria. In addition,  
<sup>193</sup> charge conjugate is always implied throughout this analysis.

## 194 7 Event Selections of DT for $\Lambda_c^+ \rightarrow nK_S^0\pi^+\pi^0$

### 195 7.1 Track Level Selection

- 196 •  $|\cos\theta| < 0.93$ ,

197 Here,  $\theta$  is the polar angle of the charged track with respect to the beam axis,  $|V_{xy}|$  and  $|V_z|$  are the  
198 closest approaches of a charged track to the interaction point in the  $Oxy$  plane and in the  $z$  position.

### 199 7.2 $K_S^0$ reconstruction

200  $K_S^0$  candidates are reconstructed via the process  $K_S^0 \rightarrow \pi^+\pi^-$

- 201 •  $\pi^\pm$  tracks are required to be within the polar angle coverage of the MDC,  $|\cos\theta| < 0.93$ .
- 202 •  $\pi^\pm$  tracks are required to be within 20 cm along the beam axis with respect to the IP,  $|V_z| < 20$  cm.  
203 And, there is no constraint for these tracks in the transverse plane.
- 204 • No PID requirements for pions
- 205 • The primary vertex fit is performed with any combinations of  $\pi^+\pi^-$  and the resulted  $\chi^2 < 100$ .  
206 The second vertex fit is further applied to suppress the mis-combination, and we require the decay  
207 length divided by the uncertainty of the decay length be larger than two,  $L/\sigma_L > 2$ , as Fig. 2.
- 208 • If the number of  $K_S^0$  candidate in an event is more than one, the largest  $L/\sigma_L$  value is selected as  
209 final state.

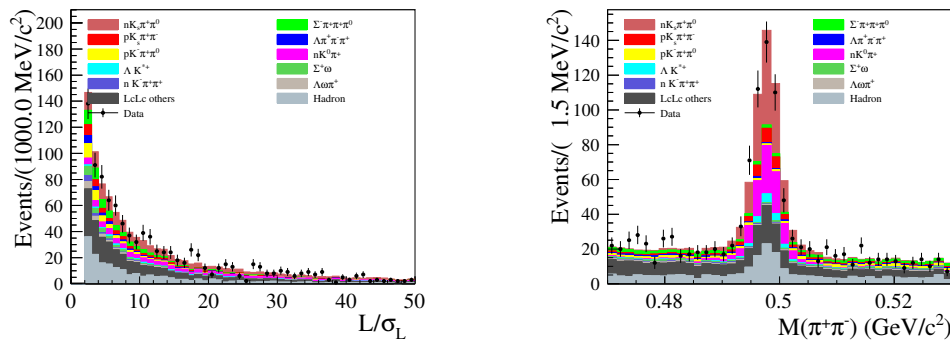


Fig. 2: Distribution of  $L/\sigma_L$  and mass of  $\pi^+\pi^-$  MC and data.

### 210 7.3 Good charged track for the bachelor $\pi^+$

211 After reconstructing  $K_S^0$ , the other  $\pi^+$  can be identified via other charged tracks. Here, We didn't  
212 require the number of additional  $\pi^-$ ,  $K^+$ , or  $K^-$ .

- 213     •  $V_{xy} < 1 \text{ cm}$ ,
- 214     •  $|V_z| < 10 \text{ cm}$ ,
- 215     •  $\pi$  PID requirements:  $\pi^+ : \mathcal{L}(\pi) > \mathcal{L}(K)$ .
- 216     • The number of  $\pi^+$  is equal to 1.

217     Here,  $\theta$  is the polar angle of the charged track with respect to the beam axis,  $V_{xy}$  and  $|V_z|$  are the  
 218     closest approaches of a charged track to the interaction point in the  $Oxy$  plane and in the  $z$  position.  
 219     Besides, the distribution other charged tracks is shown Fig. 3 (excluding  $\pi^+\pi^-$  from  $K_S^0$ ).

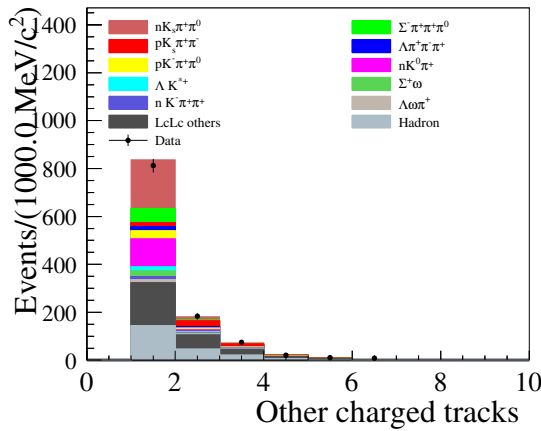


Fig. 3: Distribution of other charged tracks.

## 220     7.4 $\pi^0$ reconstruction

221      $\pi^0$  mesons are reconstructed by the decays  $\pi^0 \rightarrow \gamma\gamma$ . To reconstruct  $\pi^0$  meson, a one-constrained  
 222     (1C) kinematic fit is performed on  $\pi^0 \rightarrow \gamma\gamma$  and the invariant mass is constrained to nominal  $\pi^0$  mass.

- 223     • Photon candidates are identified using showers in the EMC. The deposited energy of each shower  
 224     must be more than 25 MeV in the barrel region ( $|\cos\theta| < 0.80$ ) and more than 50 MeV in the end  
 225     cap region ( $0.86 < |\cos\theta| < 0.92$ ).
- 226     • To suppress electronic noise and showers unrelated to the event, the difference between the EMC  
 227     time and the event start time is required to be within (0, 700) ns.
- 228     • To exclude showers that originate from charged tracks, the angle between the position of each  
 229     shower in the EMC and the closest extrapolated charged track must be greater than  $10^\circ$ .

230     • To suppress combinatorial background, we require that the  $\chi^2_{\text{IC}}$  of the kinematic fit is less than  
231       200.  $\pi^0$  candidates are reconstructed from pairs of photons whose invariant mass satisfies (0.115,  
232       0.150)  $\text{GeV}/c^2$ .

233     • If the number of  $\pi^0$  candidate in an event is more than one, the lowest  $\chi^2_{\text{IC}}$  is selected as final state.

234

235 **8 Study of backgrounds**

236 **8.1 Background analysis**

237 The kinematic variable definition:

$$M(n) = \sqrt{E(n)^2 - \vec{p}(n)^2} \quad (8)$$

238 is used to obtain the information of the undetected neutron, where  $E(n)$  and  $\vec{p}(n)$  are the missing energy  
239 and momentum carried away by the undetected neutron. For  $\Lambda_c^+ \rightarrow n K_S^0 \pi^+ \pi^0$ , the  $E(n)$  is calculated with

$$E(n) = E_{\text{beam}} - E_{K_S^0} - E_{\pi^+} - E_{\pi^0}, \quad (9)$$

240 where  $E_{\text{beam}}$  is the beam energy,  $E_{K_S^0}$ ,  $E_{\pi^+}$ , and  $E_{\pi^0}$  are the measured energies of  $K_S^0$ ,  $\pi^+$ , and  $\pi^0$  in the  
241 center-of-mass system, respectively. The  $\vec{p}(n)$  is calculated by

$$\vec{p}(n) = \vec{p}_{\Lambda_c^+} - \vec{p}_{K_S^0} - \vec{p}_{\pi^+} - \vec{p}_{\pi^0}, \quad (10)$$

242 where  $\vec{p}_{\Lambda_c^+}$ ,  $\vec{p}_{K_S^0}$ ,  $\vec{p}_{\pi^+}$  and  $\vec{p}_{\pi^0}$  are the momenta of  $\Lambda_c^+$ ,  $K_S^0$ ,  $\pi^+$  and  $\pi^0$  respectively. The momentum of  
243  $\Lambda_c^+$  is obtained by

$$\vec{p}_{\Lambda_c^+} = -\hat{p}_{\text{tag}} \sqrt{E_{\text{beam}}^2 - m_{\Lambda_c^+}^2}, \quad (11)$$

244 where  $\hat{p}_{\text{tag}}$  denotes the direction of the momentum of ST side and  $m_{\Lambda_c^+}$  is the mass of the  $\Lambda_c^+$

245 We draw main background and signal events based on the  $\Lambda_c^+$  inclusive samples and hadron sam-  
246 ples in the Fig. 4. The dominant peaking background channels are  $\Lambda_c^+ \rightarrow \Sigma^- \pi^+ \pi^+ \pi^0$  ( $n \pi^- \pi^+ \pi^+ \pi^0$ ),  
247  $\Lambda_c^+ \rightarrow \Sigma^+ \omega$  ( $n \pi^+ \pi^+ \pi^- \pi^0$ ),  $\Lambda_c^+ \rightarrow \Lambda \pi^+ \pi^+ \pi^-$  ( $n \pi^0 \pi^+ \pi^+ \pi^-$ ) and  $\Lambda_c^+ \rightarrow \Lambda K^{*+}$  ( $n \pi^0 \pi^+ \pi^+ \pi^-$ ). The detail of  
248 background channels can be found in Appendix A.6.

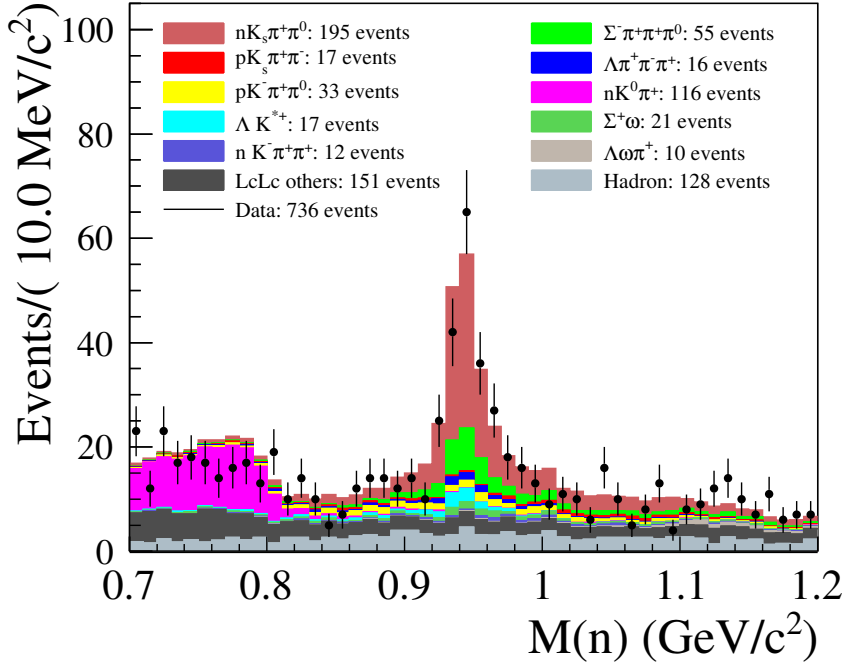


Fig. 4: Background distribution of recoil mass of  $K_S^0 \pi^+ \pi^0$  inclusive MC sample.

249 In order to remove peaking backgrounds, we apply vetoes on the defined mass spectra. We fit these  
 250 defined mass spectra, where signal and background are described by crystal ball function and Chebyshev  
 251 polynomial, respectively, and the mass windows are defined within  $3\sigma$  of crystal ball function. For  
 252  $\Sigma^- \pi^+ \pi^+ \pi^0$ , the vetoed region of  $M(n\pi^+) - M(n)$  is decided to be  $[0.23, 0.28] \text{ GeV}/c^2$ . For  $\Sigma^+ \omega$  ( $\pi^+$  from  
 253  $\Lambda_c^+$ ), the mass window of  $M(n\pi^+) - M(n)$  is chosen as  $[0.22, 0.27] \text{ GeV}/c^2$ . For  $\Sigma^+ \omega$  ( $\pi^+$  from  $K_S^0$ ), the  
 254 mass window of  $M(n\pi^-) - M(n)$  is chosen as  $[0.23, 0.28] \text{ GeV}/c^2$ . For  $\Delta \pi^+ \pi^- \pi^+$  and  $\Delta K^{*+}$ , we require  
 255  $M(n\pi^0) - M(n)$  should be larger than 0.2 GeV. The fitting results are shown in Fig. 5. The distribution  
 256 of recoil mass of  $K_S^0 \pi^+ \pi^0$  after the above vetoes is shown in Fig. 6. Here,  $M(n\pi^-)$  is recoil mass of  
 257  $\pi^+ \pi^+ \pi^0$ ,  $M(n\pi^+)$  is recoil mass of  $\pi^+ \pi^- \pi^0$ ,  $M(n\pi^0)$  is recoil mass of  $\pi^+ \pi^+ \pi^-$ , and  $M(n)$  is recoil mass of  
 258  $\pi^+ \pi^+ \pi^- \pi^0$ .

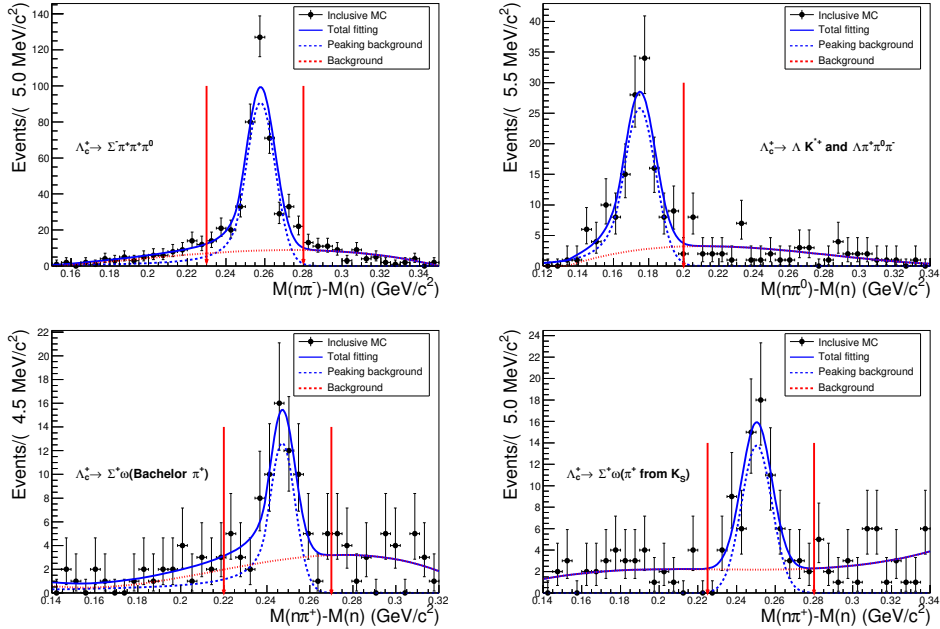


Fig. 5: The fitting of invariant mass  $M(n\pi^+) - M(n)$ ,  $M(n\pi^-) - M(n)$  and  $M(n\pi^0) - M(n)$  for peak background.

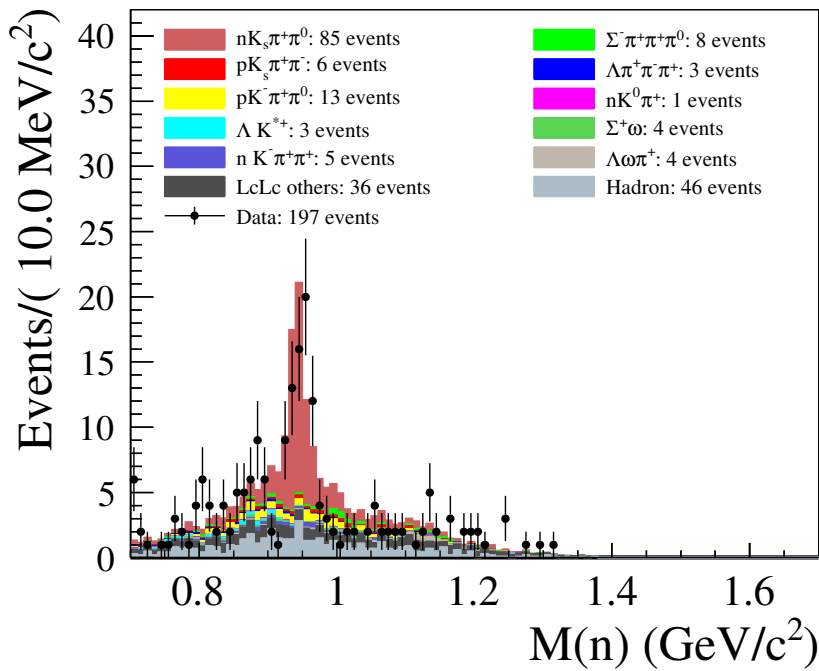


Fig. 6: Background distribution of recoil mass of  $K_S^0\pi^+\pi^0$  inclusive MC sample after vetoing peaking background.

259 **9 Branching fraction measurement**

260 **9.1 Summary of event selection criteria and cut flow**

Tab. 6: Summary of selection criteria for signal process.

Cut name	Specific cut	Relative efficiencies (%)
Good charged tracks for $K_S^0$	$ V_z  < 20 \text{ cm}, \cos \theta < 0.93$	71.3
$\pi^0$ candidate	Good photon requirement and $\pi^0$ requirement	85.9
$K_S^0$ candidate	$L/\sigma_L > 0$	74.5
Good charged tracks for $\pi^+$	$ V_z  < 10 \text{ cm},  V_r  < 1 \text{ cm}, \cos \theta < 0.93$ and Standard PID requirement	85.7
ST selections	$M_{BC}$ and $\Delta E$ requirements	55.0
Further $K_S^0$ requirement	$M(\pi^+\pi^-) \in (0.45, 0.55)\text{GeV}/c^2$ and $L/\sigma_L > 2$	79.0
Veto peaking background cut	$M(n\pi^+) - M(n), M(n\pi^-) - M(n)$ , and $M(n\pi^0) - M(n)$ requirements	43.9

261 **9.2 DT efficiency**

262 Compared with the distribution of momentum and  $\cos\theta$  of PHSP MC samples and Data, MC samples  
 263 are roughly consistent with data in momentum and  $\cos\theta$  of  $n, K_S^0, \pi^+$  and  $\pi^0$ , in Fig. 7 and 8. Therefore,  
 264 the selection efficiency is calculated by counting the numbers with PHSP MC sample and listed in Tab. 7.

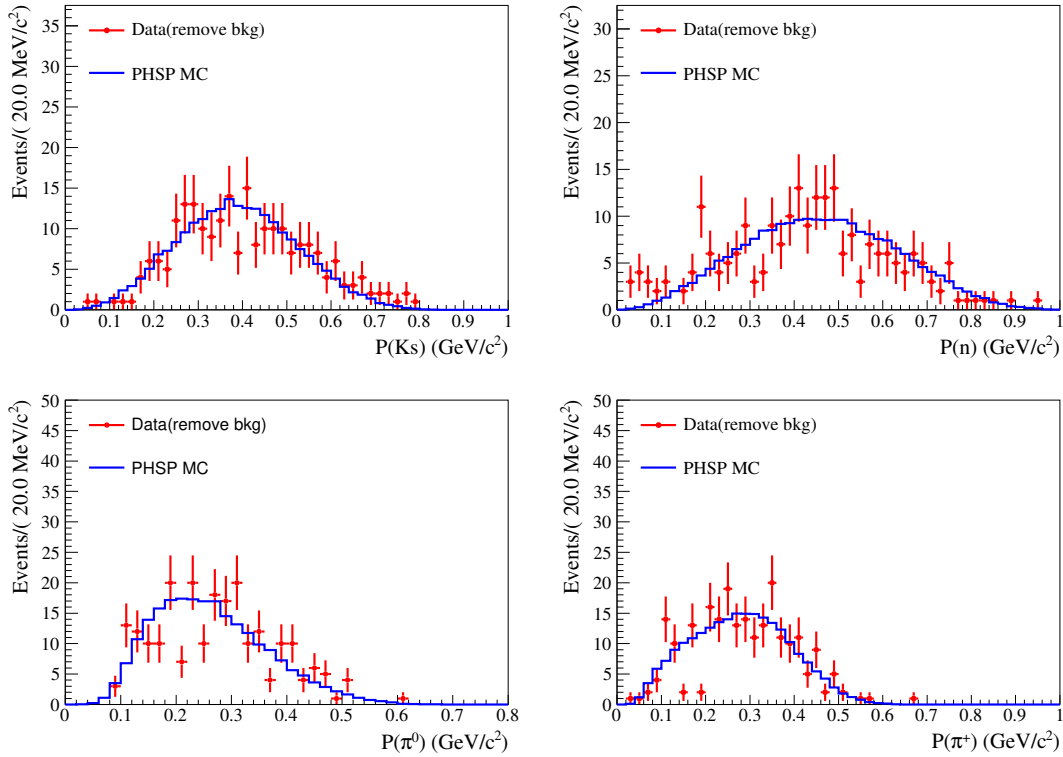
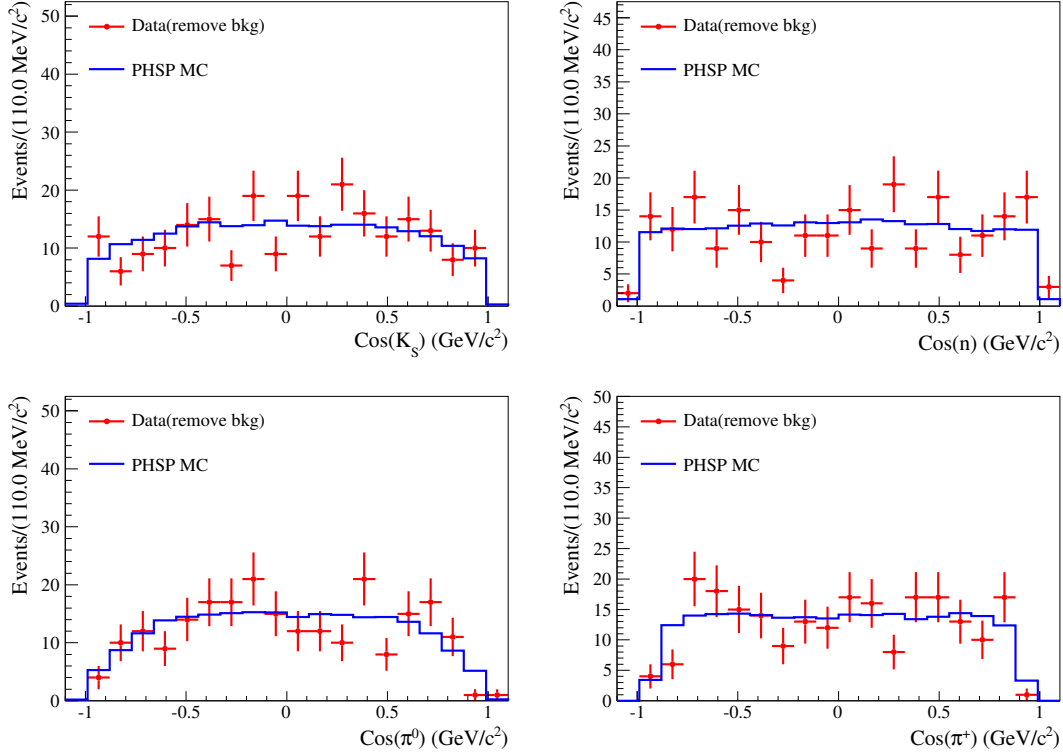


Fig. 7: The momentum distribution for final particle:  $K_S^0, n, \pi^0$ , and  $\pi^+$ .

Fig. 8: The  $\cos \theta$  distribution for final particle:  $K_S^0$ ,  $n$ ,  $\pi^0$ , and  $\pi^+$ .Tab. 7: DT efficiencies(%) which combined charge conjugation modes from  $\sqrt{s} = 4.600$  GeV to 4.699 GeV.

modes	4.600 GeV	4.612 GeV	4.628 GeV	4.641 GeV	4.661 GeV	4.682 GeV	4.699 GeV
$\bar{p}K_S^0$	$8.30 \pm 0.07$	$8.00 \pm 0.07$	$7.47 \pm 0.07$	$7.01 \pm 0.07$	$6.75 \pm 0.07$	$6.66 \pm 0.07$	$6.45 \pm 0.07$
$\bar{p}K^+\pi^-$	$8.06 \pm 0.07$	$7.30 \pm 0.07$	$7.11 \pm 0.07$	$7.03 \pm 0.07$	$6.96 \pm 0.07$	$6.59 \pm 0.07$	$6.41 \pm 0.07$
$\bar{p}K_S^0\pi^0$	$3.13 \pm 0.05$	$2.89 \pm 0.05$	$2.75 \pm 0.05$	$2.63 \pm 0.05$	$2.65 \pm 0.05$	$2.56 \pm 0.05$	$2.39 \pm 0.05$
$\bar{p}K_S^0\pi^-\pi^+$	$2.96 \pm 0.05$	$2.53 \pm 0.05$	$2.42 \pm 0.05$	$2.40 \pm 0.05$	$2.43 \pm 0.05$	$2.27 \pm 0.05$	$2.29 \pm 0.05$
$\bar{p}K^+\pi^-\pi^0$	$3.09 \pm 0.05$	$2.81 \pm 0.05$	$2.58 \pm 0.05$	$2.59 \pm 0.05$	$2.43 \pm 0.05$	$2.30 \pm 0.05$	$2.31 \pm 0.05$
$\bar{\Lambda}\pi^-$	$7.24 \pm 0.06$	$6.34 \pm 0.06$	$5.90 \pm 0.06$	$5.94 \pm 0.06$	$5.92 \pm 0.06$	$5.53 \pm 0.06$	$5.46 \pm 0.06$
$\bar{\Lambda}\pi^-\pi^0$	$2.99 \pm 0.05$	$2.67 \pm 0.04$	$2.54 \pm 0.04$	$2.34 \pm 0.04$	$2.27 \pm 0.04$	$2.27 \pm 0.04$	$2.25 \pm 0.04$
$\bar{\Lambda}\pi^-\pi^+\pi^-$	$2.04 \pm 0.04$	$1.78 \pm 0.04$	$1.74 \pm 0.04$	$1.70 \pm 0.04$	$1.68 \pm 0.04$	$1.67 \pm 0.04$	$1.69 \pm 0.04$
$\bar{\Sigma}^0\pi^-$	$4.29 \pm 0.05$	$3.75 \pm 0.05$	$3.64 \pm 0.05$	$3.53 \pm 0.05$	$3.46 \pm 0.05$	$3.34 \pm 0.05$	$3.26 \pm 0.05$
$\bar{\Sigma}^-\pi^0$	$3.52 \pm 0.05$	$3.42 \pm 0.05$	$3.15 \pm 0.05$	$3.06 \pm 0.05$	$2.82 \pm 0.05$	$2.71 \pm 0.04$	$2.58 \pm 0.04$
$\bar{\Sigma}^-\pi^-\pi^+$	$3.82 \pm 0.05$	$3.55 \pm 0.05$	$3.40 \pm 0.05$	$3.34 \pm 0.05$	$3.17 \pm 0.05$	$2.97 \pm 0.05$	$2.90 \pm 0.05$

### 265 9.3 Branching fraction

266 To obtain the signal yields, a two dimensional (recoil mass of  $K_S^0\pi^+\pi^0$  and  $M(\pi^+\pi^-)$  mass spectra)  
267 simultaneous fit method is performed on the fitting region of  $[0.7, 1.2] \times [0.47, 0.53]$   $\text{GeV}/c^2$  in the signal

268 region [2.280, 2.296]  $\text{GeV}/c^2$  and side-band region [2.250, 2.270]  $\text{GeV}/c^2$  for  $M_{BC}$  of tag side. In the  
 269 simultaneous fit, the ratio of the number of hadron background events between  $M_{BC}$  signal and side-band  
 270 region is used and it can be determined by fitting  $M_{BC}$  distribution. The method can ensure that non-  
 271  $\Lambda_c^+ \bar{\Lambda}_c^-$  pair (or  $q\bar{q}$ ) background is well estimated and is also used in previous BESIII measurement for  
 272  $\Lambda_c^+ \rightarrow n K_S^0 \pi^+$  [18]. Figure. 9 show the  $M(n)$  mass spectrum and  $M(\pi^+ \pi^-)$  mass spectrum in the  $M_{BC}$   
 273 signal and side-band region, respectively. Figure. 10 show the two dimensional mass distribution for  
 274  $M(n)$  and  $M(\pi^+ \pi^-)$  in the  $M_{BC}$  signal and side-band region, respectively.

275 The probability density functions (PDFs) of two dimensional (2D) fit are described as:

$$\begin{aligned} \text{Function}_{\text{signal region}} = & N_{\text{sig}} \times \left( \text{PDF}_{\text{sig shape}} \otimes \text{Gauss}(\mu_1, \mu_2, \sigma_1, \sigma_2) \right) + N_{\Lambda_c \text{ bkg}} \times \text{PDF}_{\Lambda_c \text{ shape}} \\ & + N_{\text{hadron bkg}} / 1.26 \times \text{PDF}_{\text{hadron}} \end{aligned} \quad (12)$$

$$\text{Function}_{\text{side-band region}} = N_{\text{hadron bkg}} \times \text{PDF}_{\text{hadron}}, \quad (13)$$

276 where  $N_{\text{sig}}$ ,  $N_{\Lambda_c \text{ bkg}}$  and  $N_{\text{hadron bkg}}$  denote signal yields,  $\Lambda_c^+ \bar{\Lambda}_c^-$  background yields and non- $\Lambda_c^+ \bar{\Lambda}_c^-$  hadron  
 277 background yields, respectively, the ratio of the number of hadron background events between  $M_{BC}$   
 278 signal and side-band region is 1.26, which can be determined by fitting  $M_{BC}$  distribution in Appendix  
 279 C of BAM-624 [25], and  $\text{Gauss}(\mu_1, \sigma_1, \mu_2, \sigma_2)$  represents 2 dimensional Gaussian function, with  $\mu$  and  
 280  $\sigma$  denoting mean and standard deviation in the Tab. 8. Here, Gaussian parameters can be obtained  
 281 by fitting data with one-dimensional fit. The correlation between  $M(n)$  and  $M(\pi^+ \pi^-)$  is calculated to  
 282 be  $\rho = 0.9831$  and considered when calculating the smearing values of  $M(n)$  and  $M(\pi^+ \pi^-)$  with the  
 283 following expressions:

$$V = \begin{bmatrix} \sigma_1^2 & \rho \sigma_1 \sigma_2 \\ \rho \sigma_1 \sigma_2 & \sigma_2^2 \end{bmatrix}, A = \sqrt{V} = \begin{bmatrix} A_{00} & A_{01} \\ A_{10} & A_{11} \end{bmatrix} = \begin{bmatrix} 3.7 \times 10^{-3} & 4.3 \times 10^{-4} \\ 4.3 \times 10^{-4} & 5.0 \times 10^{-5} \end{bmatrix},$$

$$M(n)_{\text{smearing}} = M(n) + \mu_1 + A_{00} \cdot x_1 + A_{01} \cdot x_2,$$

$$M(\pi^+ \pi^-)_{\text{smearing}} = M(\pi^+ \pi^-) + \mu_2 + A_{10} \cdot x_1 + A_{11} \cdot x_2$$

284 Here,  $\mu_1$  and  $\mu_2$  denote the shifts,  $\sigma_1$  and  $\sigma_2$  denote the smearing factors, and  $x_1$  and  $x_2$  are two numbers  
 285 which obey normal distributions  $\text{Gauss}(0, 1)$ . The detailed information can be found in Appendix.C

Tab. 8: Smear parameters

Mass spectrum	Mean ( $\text{GeV}/c^2$ )	$\sigma$ ( $\text{GeV}/c^2$ )
$M(n)$	$\mu_1 = 0.00597 \pm 0.00241$	$\sigma_1 = 0.00369 \pm 0.00480$
$M(\pi^+ \pi^-)$	$\mu_2 = -0.00028 \pm 0.01154$	$\sigma_2 = 0.00005 \pm 0.00092$

286  $PDF_{\text{hadron}}$  can be described as:

$$PDF_{\text{hadron}} = (PDF_{\text{1st cheb}} + PDF_{K_S^0 \text{ shape}}) \times PDF_{\text{1st cheb}}, \quad (14)$$

287 where  $PDF_{\text{1st cheb}}$  represents the first order Chebyshev polynomial and  $PDF_{K_S^0 \text{ shape}}$  represents signal  
288 shape of  $K_S^0$ . Here, the common parameter and  $PDF$  are  $N_{\text{hadron bkg}}$  and  $PDF_{\text{hadron}}$  in the simultaneous  
289 fit.

290 The signal PDF and the  $\Lambda_c^+ \bar{\Lambda}_c^-$  background are described with 2D MC shape, and the hadronic  
291 background is described by the events in  $M_{\text{BC}}$  side-band region. Besides, using 2D PDF, we gener-  
292 ate 200 copies of toy MC samples to confirm no bias and corresponding pull distribution is shown in the  
293 Appendix. B.

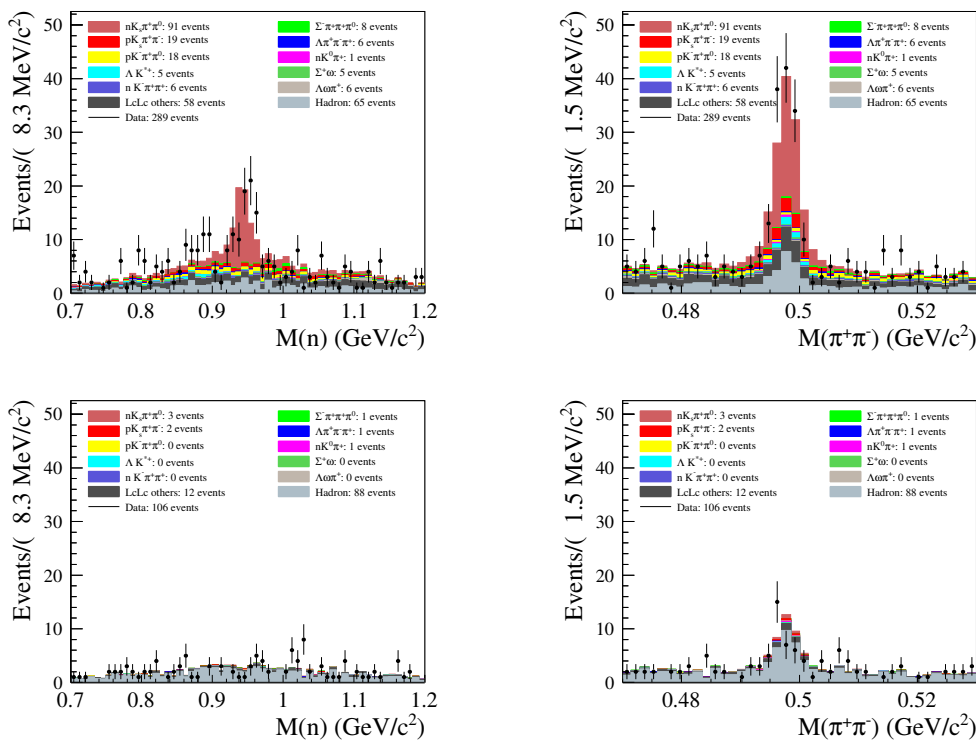


Fig. 9: The mass distribution of  $n$  and  $\pi^+ \pi^-$  for signal (upper two plots) and side-band (lower two plots) regions, respectively.

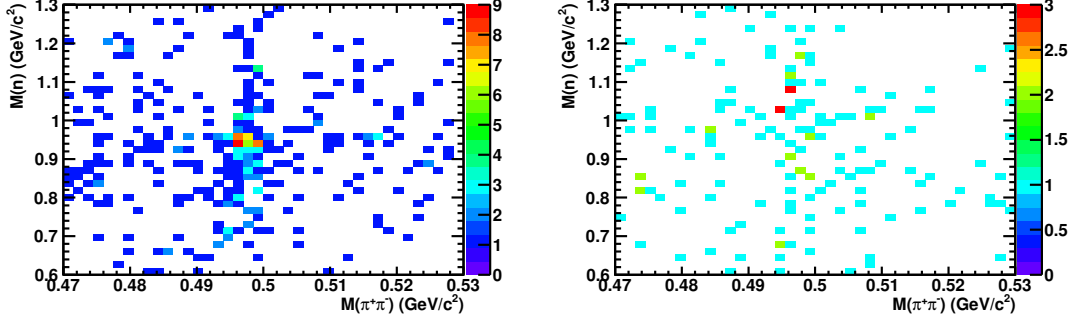


Fig. 10: The scatter plots of  $\pi^+\pi^-$  versus  $n$  for the signal (left plot) and side-band (right plot) regions.

Using the previous formulas, the fit result can be obtained and shown in the Fig. 11 (in the Fig. 31).

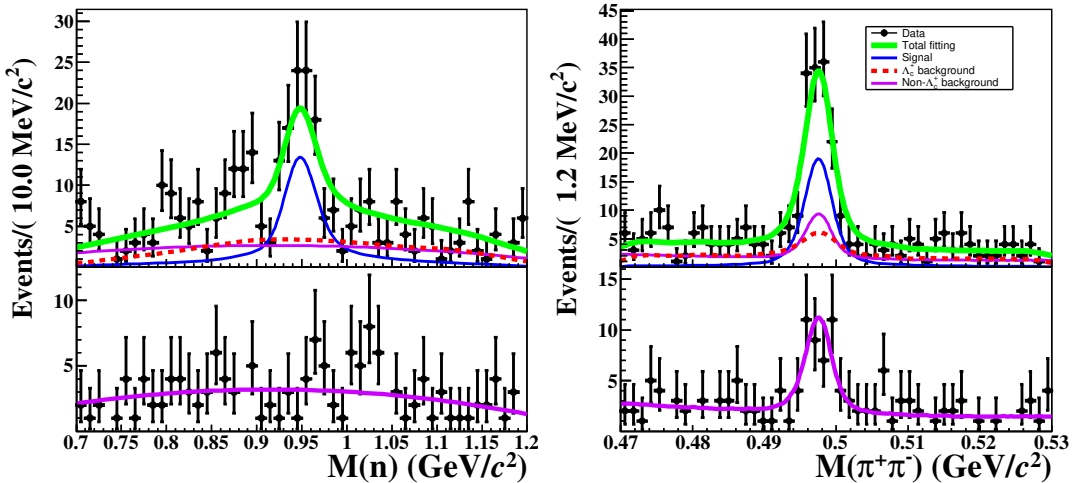


Fig. 11: 2D fit to the distributions of the invariant mass of  $n$  and  $\pi^+\pi^-$  in signal (upper two plots) and side-band (lower two plots) regions, respectively.

The branch fraction is calculated according to

$$B_{\text{final signal}} = \frac{\sum_{\alpha} N_{-,s}^{\alpha,\text{DT}}}{B_{\text{sub}} \times \sum_{\alpha} \sum_i (\frac{N_i^{\alpha,\text{ST}}}{\varepsilon_i^{\alpha,\text{ST}}} \times \varepsilon_{i,s}^{\text{DT}})} = \frac{N_{-,s}^{\text{DT}}}{B_{\text{sub}} \times \sum_{\alpha} \sum_i (\frac{N_i^{\alpha,\text{ST}}}{\varepsilon_i^{\alpha,\text{ST}}} \times \varepsilon_{i,s}^{\text{DT}})} \quad (15)$$

By comparing the Likelihood values with/without signal contribution, the FCN value changes from -3049.13 to -3006.82. The FCN value is the - log-likelihood value of the fitting result and the significance can be calculated based on  $\sqrt{2} \times (3049.13 - 3006.82) = 9.2$ . According to all the numbers above, the branching fraction can be determined and the details are listed in Tab. 9, where the first uncertainty are statistical.

Tab. 9: The branching fraction of  $\Lambda_c^+ \rightarrow n K_S^0 \pi^+ \pi^0$  process

Decay mode	Branching fraction ( $\times 10^{-2}$ )	Signal yields	Significance
$\Lambda_c^+ \rightarrow n K_S^0 \pi^+ \pi^0$	$0.85 \pm 0.13$	$98 \pm 15$	$9.2 \sigma$

## 301 10 Systematic uncertainties of branching fraction measurement

302 The uncertainties of the branching fraction measurement include the uncertainties of tracking, PID,  
 303  $\pi^0$  reconstruction,  $K_S^0$  reconstruction, branching fraction, STag  $\bar{\Lambda}_c^-$  yields, MC statistics, the fitting range,  
 304 fitting method, and veto peaking background, which are listed in the Tab 10.

Tab. 10: The total uncertainties of the branching fraction for  $\Lambda_c^+ \rightarrow nK_S^0\pi^+\pi^0$

Source	$\Lambda_c^+ \rightarrow nK_S^0\pi^+\pi^0$
Tracking and PID	0.3%
$\pi^0$ reconstruction	0.2%
$K_S^0$ reconstruction	0.9%
$Br(K_S^0 \rightarrow \pi^+\pi^-)$	0.1%
$Br(\pi^0 \rightarrow \gamma\gamma)$	negligible
Fitting model in the ST side	0.2%
MC statistics	0.4%
Fitting model	1.9%
Veto Peaking Background	0.3%
MC model	3.0%
Total	3.7%

### 305 10.1 Tracking and PID

306 For pion, the uncertainty of tracking and PID is calculated by using formula:

$$\Delta = \frac{\sum_{i=1}^N n_i \times f_{i,\text{ratio}}}{\sum_{i=1}^N n_i} \quad (16)$$

307 , where  $N$  is total number of bin for  $\pi^+$  momentum distribution,  $n_i$  represent the number of events in  $i_{\text{th}}$   
 308 bin for  $\pi^+$  momentum distribution bin, and  $f_{i,\text{ratio}}$  represent ratio of selection efficiency between data and  
 309 MC for  $\pi^+$  momentum distribution. So, systematic uncertainty from  $\pi^+$  is calculated to be 0.3%. detailed  
 310 information of ratio can be found in the Ref. [19].

### 311 10.2 $\pi^0$ reconstruction

312 The uncertainty of  $\pi^0$  reconstruction is calculated by using formula:

$$\Delta = \frac{\sum_{i=1}^N n_i \times f_{i,\text{ratio}}}{\sum_{i=1}^N n_i} \quad (17)$$

313 , where  $N$  is total number of bin for  $\pi^0$  momentum distribution,  $n_i$  represent the number of events in  $i_{\text{th}}$   
 314 bin for  $\pi^0$  momentum distribution bin, and  $f_{i,\text{ratio}}$  represent ratio of selection efficiency between data and  
 315 MC for  $\pi^0$  momentum distribution. So, systematic uncertainty from  $\pi^0$  is calculated to be 0.2%. detailed  
 316 information of ratio can be found in the Ref. [20].

317    **10.3  $K_S^0$  reconstruction**

318    The uncertainty of  $K_S^0$  reconstruction is calculated by using formula:

$$\Delta = \frac{\sum_{i=1}^N n_i \times f_{i,\text{ratio}}}{\sum_{i=1}^N n_i} \quad (18)$$

319 , where  $N$  is total number of bin for  $K_S^0$  momentum distribution,  $n_i$  represent the number of events in  
 320  $i$ <sub>th</sub> bin for  $K_S^0$  momentum distribution bin, and  $f_{i,\text{ratio}}$  represent ratio of selection efficiency between data  
 321 and MC for  $K_S^0$  momentum distribution. So, systematic uncertainty from  $K_S^0$  is calculated to be 0.9%.  
 322 detailed information of ratio can be found in the Ref. [21].

323    **10.4 Branching fraction**

324    The  $Br(\pi^0 \rightarrow \gamma\gamma) = (98.823 \pm 0.034)\%$  is from PDG [23], the uncertainty is assigned to be 0.03%  
 325 and the  $Br(K_S^0 \rightarrow \pi^+\pi^-) = (69.20 \pm 0.05)\%$  is from PDG, the uncertainty is assigned to be 0.1%.

326    **10.5 Fitting model in the ST side**

327    The systematic uncertainty of this term is quoted from Ref. [5], which is 0.2%.

328    **10.6 MC statistics**

329    In the analysis, ST yields, DT efficiencies, and ST efficiencies all include statistical uncertainties.  
 330 The systematic uncertainty caused by the input ST yields, DT efficiencies, and ST efficiencies are 0.36%,  
 331 0.24%, and 0.06%. So, the total uncertainty is assigned to be 0.4%.

332    **10.7 Fitting model**

- 333    • For 2D signal shape: To estimate the uncertainties of 2D signal shape, we use two Gaussian func-  
 334    tions to describe signal contribution and taken the change of the result as systematic uncertainty,  
 335    which is 0.6%.

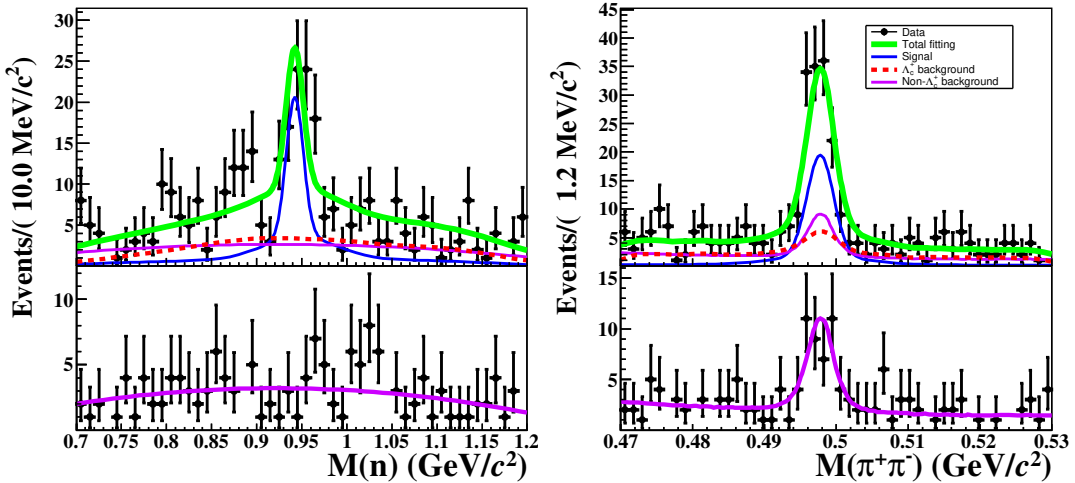


Fig. 12: 2D fit to the distributions of the invariant mass of  $n$  and  $\pi^+\pi^-$  in signal (upper two plots) and side-band (lower two plots) regions, respectively.

- 336 • To estimate the systematic uncertainty caused by this ratio  $1.26 \pm 0.005$ , which can be determined  
 337 by fitting  $M_{BC}$  in Appendix C of MEMO-624 [25], we float the ratio with  $1\sigma$ , the difference be-  
 338 tween the measured branching fractions using different ratios is assigned as systematic uncertainty  
 339 in the Fig. 13. Given that the uncertainty of the ratio is quite small, the systematic uncertainty of  
 340 this term is decided to be negligible.

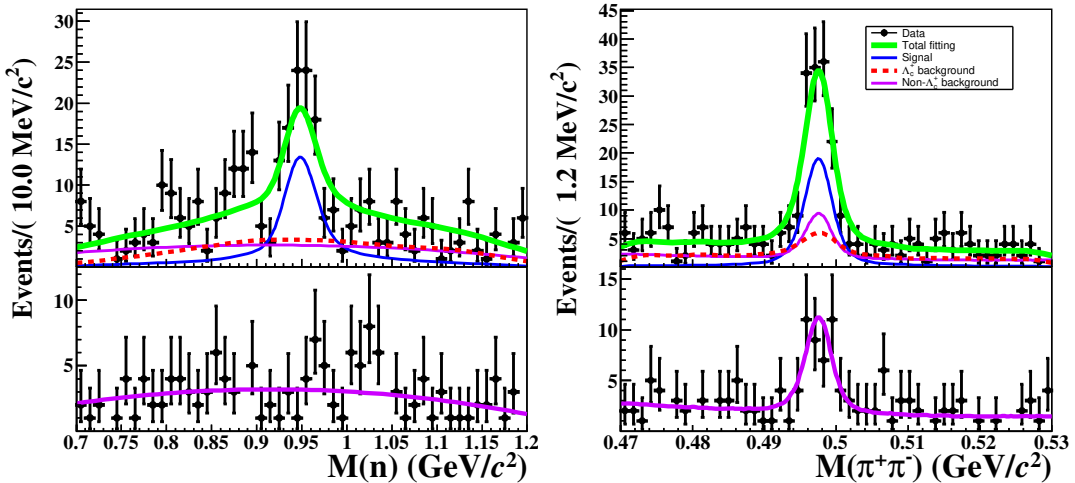


Fig. 13: 2D fit to the distributions of the invariant mass of  $n$  and  $\pi^+\pi^-$  in signal (upper two plots) and side-band (lower two plots) regions, respectively.

- 341 • For the shape of  $\Lambda_c^+$  background contribution, changing the smoothness of the shape (The coeffi-

342 client value of Keyspdf is from 1 to 2) in the Fig. 14, the differences are taken as the systematic  
 343 uncertainties, which is 1.8%.

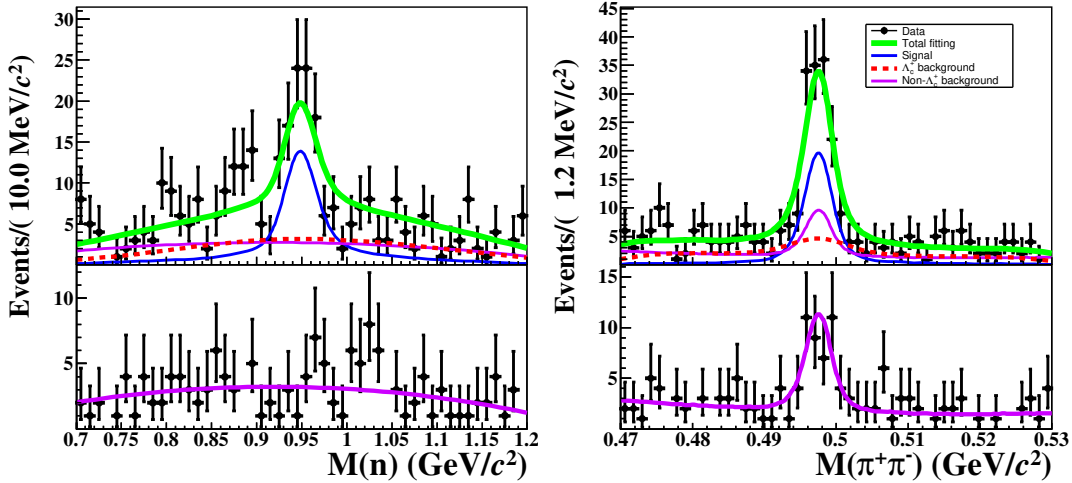


Fig. 14: 2D fit to the distributions of the invariant mass of  $n$  and  $\pi^+\pi^-$  in signal (upper two plots) and side-band (lower two plots) regions, respectively.

- 344 • To estimate the systematic uncertainty caused by those parameters, we float the ratio with  $1\sigma$ , the  
 345 difference between the measured branching fractions using different ratios is assigned as system-  
 346 atic uncertainty in the Fig. 15. Given that the uncertainty of the ratio is quite small, the systematic  
 347 uncertainty of this term is decided to be negligible.

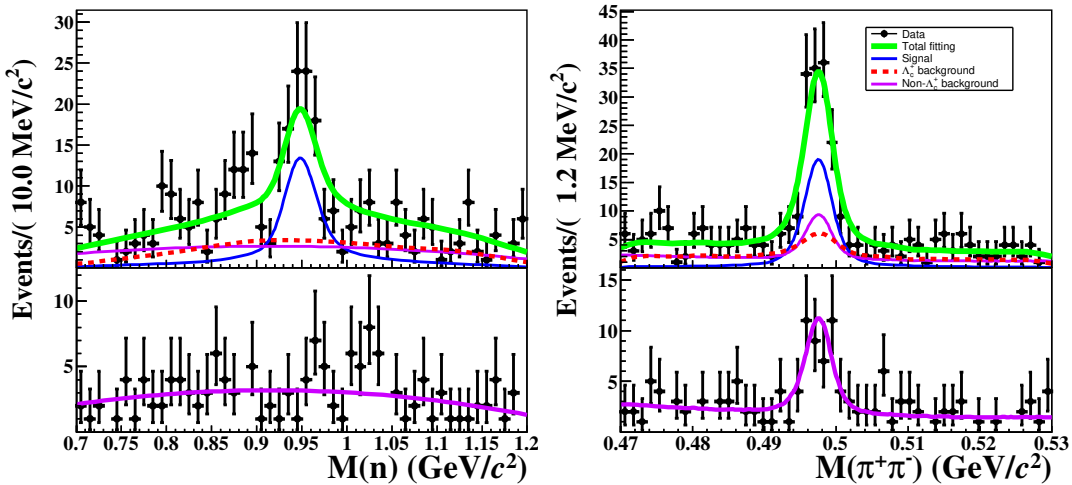


Fig. 15: 2D fit to the distributions of the invariant mass of  $n$  and  $\pi^+\pi^-$  in signal (upper two plots) and side-band (lower two plots) regions, respectively.

### 348 10.8 Veto peaking background

349 We use control samples  $\Lambda_c^+ \rightarrow \Sigma^+ (n\pi^+) \pi^+ \pi^-$ ,  $\Lambda_c^+ \rightarrow \Sigma^- (n\pi^-) \pi^+ \pi^+$  and  $\Lambda_c^+ \rightarrow \Lambda^+ (n\pi^0) \pi^+$  to study  
 350 systematic uncertainty by smearing signal MC sample with the Gaussian function to calculate new ef-  
 351 ficiency and take the difference of branching fraction as systematic uncertainty, which are about 0.1%,  
 352 0.1% and 0.2%. Here, Gaussian parameters are shown in the Tab. 11 and new efficiencies are shown in  
 353 the Tab. 12, Tab. 13, and Tab. 14, where Gaussian parameters of control samples  $\Lambda_c^+ \rightarrow \Sigma^+ (n\pi^+) \pi^+ \pi^-$   
 354 and  $\Lambda_c^+ \rightarrow \Sigma^- (n\pi^-) \pi^+ \pi^+$  are quoted from BAM-624 [25] and Gaussian parameters of control sample  
 355  $\Lambda_c^+ \rightarrow \Lambda^+ (n\pi^0) \pi^+$  can be obtained fitting data with MC shape convoluted Gaussian parameter in the  
 356 Appendix A.5.

Tab. 11: The information of different control samples

Control sample	Mean (GeV/c <sup>2</sup> )	$\sigma$ (GeV/c <sup>2</sup> )
$\Lambda_c^+ \rightarrow \Sigma^+ (n\pi^+) \pi^+ \pi^-$	$0.000031 \pm 0.000306$	$0.000151 \pm 0.000986$
$\Lambda_c^+ \rightarrow \Sigma^- (n\pi^-) \pi^+ \pi^+$	$0.000011 \pm 0.000113$	$0.000128 \pm 0.000869$
$\Lambda_c^+ \rightarrow \Lambda^+ (n\pi^0) \pi^+$	$-0.001172 \pm 0.000401$	$0.000465 \pm 0.000172$

Tab. 12: New DT efficiencies(%) which combined charge conjugation modes from  $\sqrt{s} = 4.600$  GeV to 4.699 GeV using control samples  $\Lambda_c^+ \rightarrow \Sigma^+ (n\pi^+) \pi^+ \pi^-$ .

modes	4.600 GeV	4.612 GeV	4.628 GeV	4.641 GeV	4.661 GeV	4.682 GeV	4.699 GeV
$\bar{p}K_S^0$	$7.08 \pm 0.07$	$6.30 \pm 0.07$	$6.01 \pm 0.07$	$5.96 \pm 0.07$	$5.82 \pm 0.07$	$5.67 \pm 0.07$	$5.48 \pm 0.07$
$\bar{p}K^+\pi^-$	$6.82 \pm 0.07$	$6.17 \pm 0.07$	$6.00 \pm 0.07$	$5.96 \pm 0.07$	$5.82 \pm 0.07$	$5.67 \pm 0.07$	$5.38 \pm 0.07$
$\bar{p}K_S^0\pi^0$	$2.80 \pm 0.05$	$2.48 \pm 0.05$	$2.29 \pm 0.05$	$2.25 \pm 0.05$	$2.24 \pm 0.05$	$2.21 \pm 0.05$	$2.06 \pm 0.05$
$\bar{p}K_S^0\pi^-\pi^+$	$2.50 \pm 0.05$	$2.13 \pm 0.05$	$2.03 \pm 0.05$	$2.00 \pm 0.05$	$2.00 \pm 0.05$	$1.90 \pm 0.05$	$1.91 \pm 0.05$
$\bar{p}K^+\pi^-\pi^0$	$2.63 \pm 0.05$	$2.30 \pm 0.05$	$2.17 \pm 0.05$	$2.13 \pm 0.05$	$2.05 \pm 0.05$	$1.95 \pm 0.05$	$1.93 \pm 0.05$
$\bar{\Lambda}\pi^-$	$6.17 \pm 0.06$	$5.36 \pm 0.06$	$4.94 \pm 0.06$	$5.03 \pm 0.06$	$4.97 \pm 0.06$	$4.70 \pm 0.06$	$4.61 \pm 0.06$
$\bar{\Lambda}\pi^-\pi^0$	$2.55 \pm 0.05$	$2.27 \pm 0.05$	$2.12 \pm 0.05$	$1.96 \pm 0.05$	$1.94 \pm 0.05$	$1.90 \pm 0.05$	$1.91 \pm 0.05$
$\bar{\Lambda}\pi^-\pi^+\pi^-$	$1.72 \pm 0.04$	$1.46 \pm 0.04$	$1.46 \pm 0.04$	$1.43 \pm 0.04$	$1.41 \pm 0.04$	$1.42 \pm 0.04$	$1.43 \pm 0.04$
$\bar{\Sigma}^0\pi^-$	$3.68 \pm 0.05$	$3.23 \pm 0.05$	$3.08 \pm 0.05$	$3.00 \pm 0.05$	$2.90 \pm 0.05$	$2.86 \pm 0.05$	$2.74 \pm 0.05$
$\bar{\Sigma}^-\pi^0$	$2.99 \pm 0.05$	$2.77 \pm 0.05$	$2.55 \pm 0.05$	$2.61 \pm 0.05$	$2.39 \pm 0.05$	$2.31 \pm 0.05$	$2.15 \pm 0.05$
$\bar{\Sigma}^-\pi^-\pi^+$	$3.22 \pm 0.05$	$2.96 \pm 0.05$	$2.83 \pm 0.05$	$2.71 \pm 0.05$	$2.64 \pm 0.05$	$2.50 \pm 0.05$	$2.40 \pm 0.05$

Tab. 13: New DT efficiencies(%) which combined charge conjugation modes from  $\sqrt{s} = 4.600$  GeV to 4.699 GeV using control samples  $\Lambda_c^+ \rightarrow \Sigma^- (n\pi^-)\pi^+\pi^+$ .

modes	4.600 GeV	4.612 GeV	4.628 GeV	4.641 GeV	4.661 GeV	4.682 GeV	4.699 GeV
$\bar{p}K_S^0$	$7.08 \pm 0.07$	$6.30 \pm 0.07$	$6.01 \pm 0.07$	$5.96 \pm 0.07$	$5.82 \pm 0.07$	$5.67 \pm 0.07$	$5.48 \pm 0.07$
$\bar{p}K^+\pi^-$	$6.82 \pm 0.07$	$6.17 \pm 0.07$	$6.00 \pm 0.07$	$5.96 \pm 0.07$	$5.82 \pm 0.07$	$5.67 \pm 0.07$	$5.39 \pm 0.07$
$\bar{p}K_S^0\pi^0$	$2.80 \pm 0.05$	$2.48 \pm 0.05$	$2.29 \pm 0.05$	$2.25 \pm 0.05$	$2.24 \pm 0.05$	$2.21 \pm 0.05$	$2.06 \pm 0.05$
$\bar{p}K_S^0\pi^-\pi^+$	$2.50 \pm 0.05$	$2.13 \pm 0.05$	$2.03 \pm 0.05$	$2.00 \pm 0.05$	$2.00 \pm 0.05$	$1.90 \pm 0.05$	$1.91 \pm 0.05$
$\bar{p}K^+\pi^-\pi^0$	$2.63 \pm 0.05$	$2.29 \pm 0.05$	$2.17 \pm 0.05$	$2.13 \pm 0.05$	$2.05 \pm 0.05$	$1.95 \pm 0.05$	$1.93 \pm 0.05$
$\bar{\Lambda}\pi^-$	$6.17 \pm 0.05$	$5.36 \pm 0.05$	$4.94 \pm 0.05$	$5.03 \pm 0.05$	$4.97 \pm 0.05$	$4.70 \pm 0.05$	$4.61 \pm 0.05$
$\bar{\Lambda}\pi^-\pi^0$	$2.55 \pm 0.05$	$2.27 \pm 0.05$	$2.12 \pm 0.05$	$1.96 \pm 0.05$	$1.94 \pm 0.05$	$1.90 \pm 0.05$	$1.91 \pm 0.05$
$\bar{\Lambda}\pi^-\pi^+\pi^-$	$1.72 \pm 0.04$	$1.46 \pm 0.04$	$1.45 \pm 0.04$	$1.43 \pm 0.04$	$1.41 \pm 0.04$	$1.42 \pm 0.04$	$1.43 \pm 0.04$
$\bar{\Sigma}^0\pi^-$	$3.68 \pm 0.05$	$3.23 \pm 0.05$	$3.08 \pm 0.05$	$3.00 \pm 0.05$	$2.90 \pm 0.05$	$2.86 \pm 0.05$	$2.74 \pm 0.05$
$\bar{\Sigma}^-\pi^0$	$2.99 \pm 0.05$	$2.77 \pm 0.05$	$2.55 \pm 0.05$	$2.61 \pm 0.05$	$2.39 \pm 0.05$	$2.31 \pm 0.05$	$2.15 \pm 0.05$
$\bar{\Sigma}^-\pi^-\pi^+$	$3.22 \pm 0.05$	$2.96 \pm 0.05$	$2.83 \pm 0.05$	$2.71 \pm 0.05$	$2.64 \pm 0.05$	$2.50 \pm 0.05$	$2.40 \pm 0.05$

Tab. 14: New DT efficiencies(%) which combined charge conjugation modes from  $\sqrt{s} = 4.600$  GeV to 4.699 GeV using control samples  $\Lambda_c^+ \rightarrow \Lambda^+ (n\pi^0)\pi^+$ .

modes	4.600 GeV	4.612 GeV	4.628 GeV	4.641 GeV	4.661 GeV	4.682 GeV	4.699 GeV
$\bar{p}K_S^0$	$7.08 \pm 0.07$	$6.30 \pm 0.07$	$5.94 \pm 0.07$	$5.99 \pm 0.07$	$5.82 \pm 0.07$	$5.63 \pm 0.07$	$5.49 \pm 0.07$
$\bar{p}K^+\pi^-$	$6.82 \pm 0.07$	$6.17 \pm 0.07$	$6.00 \pm 0.07$	$5.96 \pm 0.07$	$5.82 \pm 0.07$	$5.67 \pm 0.07$	$5.38 \pm 0.07$
$\bar{p}K_S^0\pi^0$	$2.79 \pm 0.05$	$2.48 \pm 0.05$	$2.29 \pm 0.05$	$2.25 \pm 0.05$	$2.24 \pm 0.05$	$2.21 \pm 0.05$	$2.06 \pm 0.05$
$\bar{p}K_S^0\pi^-\pi^+$	$2.51 \pm 0.05$	$2.13 \pm 0.05$	$2.03 \pm 0.05$	$2.00 \pm 0.05$	$2.00 \pm 0.05$	$1.90 \pm 0.05$	$1.91 \pm 0.05$
$\bar{p}K^+\pi^-\pi^0$	$2.63 \pm 0.04$	$2.30 \pm 0.04$	$2.17 \pm 0.04$	$2.13 \pm 0.04$	$2.05 \pm 0.04$	$1.95 \pm 0.04$	$1.93 \pm 0.04$
$\bar{\Lambda}\pi^-$	$6.17 \pm 0.05$	$5.36 \pm 0.05$	$4.94 \pm 0.05$	$5.03 \pm 0.05$	$4.97 \pm 0.05$	$4.70 \pm 0.05$	$4.61 \pm 0.05$
$\bar{\Lambda}\pi^-\pi^0$	$2.56 \pm 0.05$	$2.27 \pm 0.05$	$2.12 \pm 0.05$	$1.96 \pm 0.05$	$1.94 \pm 0.05$	$1.90 \pm 0.05$	$1.91 \pm 0.05$
$\bar{\Lambda}\pi^-\pi^+\pi^-$	$1.72 \pm 0.04$	$1.47 \pm 0.04$	$1.45 \pm 0.04$	$1.43 \pm 0.04$	$1.41 \pm 0.04$	$1.42 \pm 0.04$	$1.43 \pm 0.04$
$\bar{\Sigma}^0\pi^-$	$3.68 \pm 0.05$	$3.28 \pm 0.05$	$3.08 \pm 0.05$	$3.00 \pm 0.05$	$3.00 \pm 0.05$	$2.86 \pm 0.05$	$2.74 \pm 0.05$
$\bar{\Sigma}^-\pi^0$	$2.99 \pm 0.05$	$2.78 \pm 0.05$	$2.54 \pm 0.05$	$2.61 \pm 0.05$	$2.39 \pm 0.05$	$2.31 \pm 0.05$	$2.15 \pm 0.05$
$\bar{\Sigma}^-\pi^-\pi^+$	$3.22 \pm 0.05$	$2.96 \pm 0.05$	$2.83 \pm 0.05$	$2.71 \pm 0.05$	$2.64 \pm 0.05$	$2.50 \pm 0.05$	$2.40 \pm 0.05$

357 By fitting  $\pi^+\pi^-$  and  $n$  mass distribution from  $\Lambda_c^+ \rightarrow nK_S^0\pi^+\pi^0$  decay channel, the Gaussian parameter  
 358 can be obtained. Then, we use smearing signal MC sample with the Gaussian function to calculate new  
 359 efficiency in the Tab. 15 and take the difference of branching fraction as systematic uncertainty from  
 360 signal efficiency losing, which is about 0.1%.

Tab. 15: New DT efficiencies(%) which combined charge conjugation modes from  $\sqrt{s} = 4.600$  GeV to 4.699 GeV using control samples  $\Lambda_c^+ \rightarrow nK_S^0\pi^+\pi^0$ .

modes	4.600 GeV	4.612 GeV	4.628 GeV	4.641 GeV	4.661 GeV	4.682 GeV	4.699 GeV
$\bar{p}K_S^0$	$7.08 \pm 0.07$	$6.30 \pm 0.07$	$5.94 \pm 0.07$	$5.99 \pm 0.07$	$5.82 \pm 0.07$	$5.63 \pm 0.07$	$5.49 \pm 0.07$
$\bar{p}K^+\pi^-$	$6.82 \pm 0.07$	$6.17 \pm 0.07$	$6.00 \pm 0.07$	$5.96 \pm 0.07$	$5.82 \pm 0.07$	$5.67 \pm 0.07$	$5.38 \pm 0.07$
$\bar{p}K_S^0\pi^0$	$2.79 \pm 0.05$	$2.48 \pm 0.05$	$2.29 \pm 0.05$	$2.25 \pm 0.05$	$2.24 \pm 0.05$	$2.21 \pm 0.05$	$2.06 \pm 0.05$
$\bar{p}K_S^0\pi^-\pi^+$	$2.51 \pm 0.05$	$2.13 \pm 0.05$	$2.03 \pm 0.05$	$2.00 \pm 0.05$	$2.00 \pm 0.05$	$1.90 \pm 0.05$	$1.91 \pm 0.05$
$\bar{p}K^+\pi^-\pi^0$	$2.63 \pm 0.05$	$2.30 \pm 0.05$	$2.17 \pm 0.05$	$2.13 \pm 0.05$	$2.05 \pm 0.05$	$1.95 \pm 0.05$	$1.93 \pm 0.05$
$\bar{\Lambda}\pi^-$	$6.17 \pm 0.06$	$5.36 \pm 0.06$	$4.94 \pm 0.06$	$5.03 \pm 0.06$	$4.97 \pm 0.06$	$4.70 \pm 0.06$	$4.61 \pm 0.06$
$\bar{\Lambda}\pi^-\pi^0$	$2.56 \pm 0.05$	$2.27 \pm 0.05$	$2.12 \pm 0.05$	$1.96 \pm 0.05$	$1.94 \pm 0.05$	$1.90 \pm 0.05$	$1.91 \pm 0.05$
$\bar{\Lambda}\pi^-\pi^+\pi^-$	$1.72 \pm 0.04$	$1.47 \pm 0.04$	$1.45 \pm 0.04$	$1.43 \pm 0.04$	$1.41 \pm 0.04$	$1.42 \pm 0.04$	$1.43 \pm 0.04$
$\bar{\Sigma}^0\pi^-$	$3.68 \pm 0.05$	$3.28 \pm 0.05$	$3.08 \pm 0.05$	$3.00 \pm 0.05$	$3.00 \pm 0.05$	$2.86 \pm 0.05$	$2.74 \pm 0.05$
$\bar{\Sigma}^-\pi^0$	$2.99 \pm 0.05$	$2.78 \pm 0.05$	$2.54 \pm 0.05$	$2.61 \pm 0.05$	$2.39 \pm 0.05$	$2.31 \pm 0.05$	$2.15 \pm 0.05$
$\bar{\Sigma}^-\pi^-\pi^+$	$3.22 \pm 0.05$	$2.96 \pm 0.05$	$2.83 \pm 0.05$	$2.71 \pm 0.05$	$2.64 \pm 0.05$	$2.50 \pm 0.05$	$2.40 \pm 0.05$

## 361 10.9 MC Model

362 For the Cabibbo-Favored process  $\Lambda_c^+ \rightarrow nK_S^0\pi^+\pi^0$ , the result of reweighted signal MC is taken as  
363 nominal value. In order to consider systematic uncertainty of the MC model, the PHSP MC method is  
364 used, and difference between new branching fraction and nominal value is estimated as systematic un-  
365 certainty. Here, new efficiencies are shown in the Tab. 16. Compared with the distribution of momentum  
366 of MC and Data, the reweighted MC samples are consistent with data in momentum of  $n$ ,  $K_S^0$ ,  $\pi^+$  and  $\pi^0$   
367 and  $n\pi^+\pi^0$  mass distribution, in Fig. 16.

368 For the five distributions in different bins: the momentum  $p(K_S)$ ,  $p(n)$ ,  $p(\pi^0)$ ,  $p(\pi^+)$  and invariant  
369 mass  $M(n\pi^+\pi^0)$ , the difference factor between data and MC samples can be determined using

$$f_{k,K_S^0} = \frac{n_{i,K_S^0}^{\text{Data}}}{n_{i,K_S^0}^{\text{MC}_{\text{rec}}}}, f_{k,n} = \frac{n_{i,n}^{\text{Data}}}{n_{i,n}^{\text{MC}_{\text{rec}}}}, f_{k,\pi^0} = \frac{n_{i,\pi^0}^{\text{Data}}}{n_{i,\pi^0}^{\text{MC}_{\text{rec}}}}, f_{k,\pi^+} = \frac{n_{i,\pi^+}^{\text{Data}}}{n_{i,\pi^+}^{\text{MC}_{\text{rec}}}}, f_{k,n\pi^+\pi^0} = \frac{n_{i,n\pi^+\pi^0}^{\text{Data}}}{n_{i,n\pi^+\pi^0}^{\text{MC}_{\text{rec}}}}, \quad (19)$$

370 where  $k$  is the index for each event,  $n_{i,K_S^0}^{\text{Data}}$ ,  $n_{i,n}^{\text{Data}}$ ,  $n_{i,\pi^0}^{\text{Data}}$ ,  $n_{i,\pi^+}^{\text{Data}}$ , and  $n_{i,n\pi^+\pi^0}^{\text{Data}}$  represent the number of events  
371 in  $i$ -th bin for  $K_S^0$ ,  $n$ ,  $\pi^+$ ,  $\pi^0$ , and  $n\pi^+\pi^0$  data distribution, and  $n_{i,K_S^0}^{\text{MC}_{\text{rec}}}$ ,  $n_{i,n}^{\text{MC}_{\text{rec}}}$ ,  $n_{i,\pi^0}^{\text{MC}_{\text{rec}}}$ ,  $n_{i,\pi^+}^{\text{MC}_{\text{rec}}}$ , and  $n_{i,n\pi^+\pi^0}^{\text{MC}_{\text{rec}}}$   
372 represent the number of events in  $i$ -th bin for the reconstruction  $K_S^0$ ,  $n$ ,  $\pi^+$ ,  $\pi^0$ , and  $n\pi^+\pi^0$  MC dsitribution.

373 The efficiencies from the reweighted MC are calculated as:

$$\varepsilon_{\text{reweight}} = \frac{\sum_{k=1}^{N_{\text{rec}}} f_{k,K_S^0} \times f_{k,n} \times f_{k,\pi^0} \times f_{k,\pi^+} \times f_{k,n\pi^+\pi^0}}{\sum_{k=1}^{N_{\text{truth}}} f_{k,K_S^0} \times f_{k,n} \times f_{k,\pi^0} \times f_{k,\pi^+} \times f_{k,n\pi^+\pi^0}}, \quad (20)$$

374 where  $N_{\text{rec}}$  and  $N_{\text{truth}}$  denote the number of reconstruction and truth level MC sample, respectively.

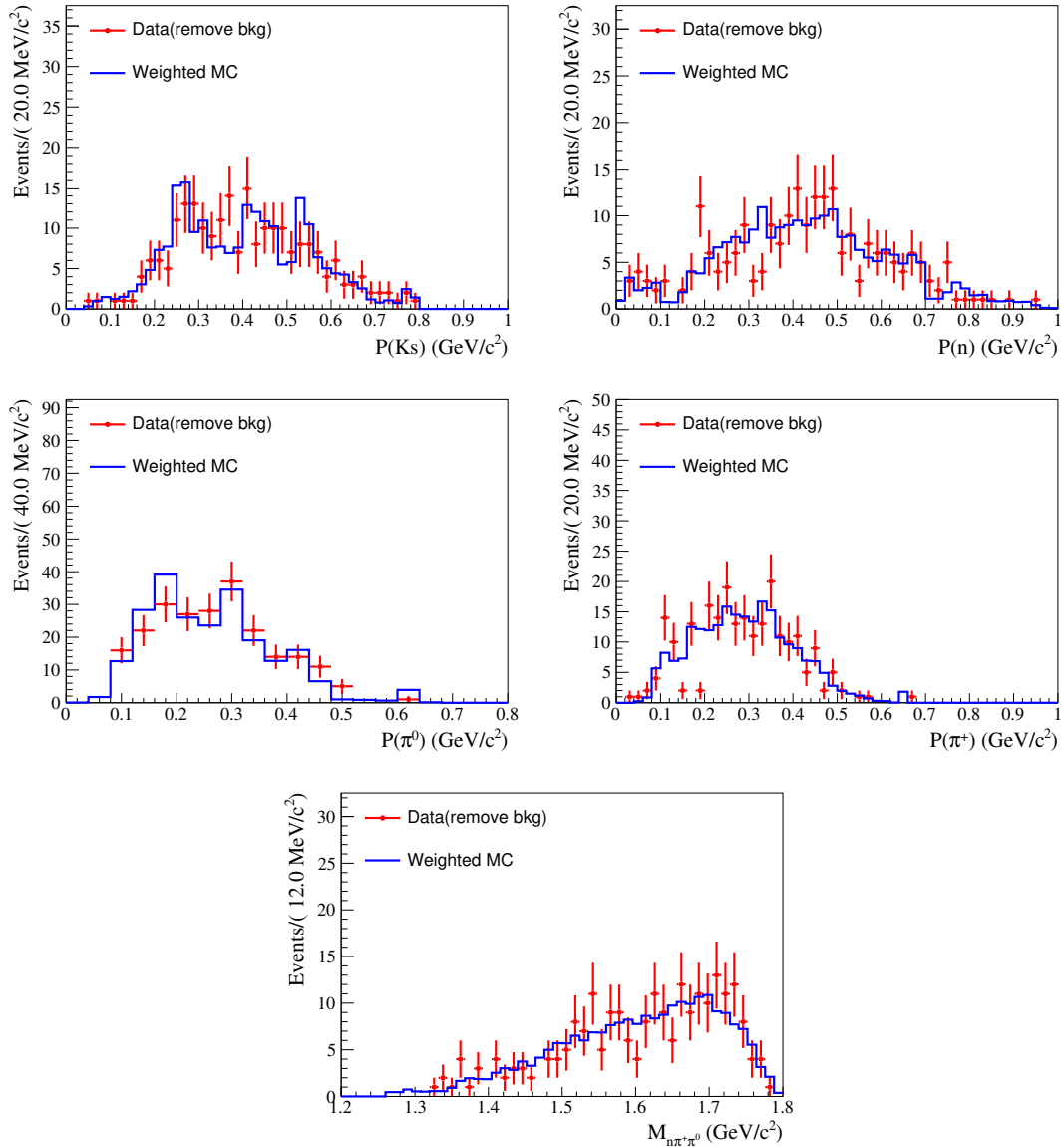


Fig. 16: The comparison of momentum and invariant mass distribution using reweighted MC method.

Tab. 16: New DT efficiencies(%) which combined charge conjugation modes from  $\sqrt{s} = 4.600$  GeV to 4.699 GeV using weight method.

modes	4.600 GeV	4.612 GeV	4.628 GeV	4.641 GeV	4.661 GeV	4.682 GeV	4.699 GeV
$\bar{p}K_S^0$	$7.12 \pm 0.07$	$6.33 \pm 0.07$	$5.96 \pm 0.07$	$6.01 \pm 0.07$	$5.74 \pm 0.07$	$5.65 \pm 0.07$	$5.51 \pm 0.07$
$\bar{p}K^+\pi^-$	$6.85 \pm 0.07$	$6.19 \pm 0.07$	$6.03 \pm 0.07$	$5.98 \pm 0.07$	$5.84 \pm 0.07$	$5.70 \pm 0.07$	$5.40 \pm 0.07$
$\bar{p}K_S^0\pi^0$	$2.81 \pm 0.05$	$2.49 \pm 0.05$	$2.30 \pm 0.05$	$2.26 \pm 0.05$	$2.24 \pm 0.05$	$2.22 \pm 0.05$	$2.06 \pm 0.05$
$\bar{p}K_S^0\pi^-\pi^+$	$2.51 \pm 0.05$	$2.13 \pm 0.05$	$2.03 \pm 0.05$	$2.00 \pm 0.05$	$2.00 \pm 0.05$	$1.90 \pm 0.05$	$1.91 \pm 0.05$
$\bar{p}K^+\pi^-\pi^0$	$2.64 \pm 0.05$	$2.30 \pm 0.05$	$2.18 \pm 0.05$	$2.14 \pm 0.05$	$2.05 \pm 0.05$	$1.96 \pm 0.05$	$1.93 \pm 0.05$
$\bar{\Lambda}\pi^-$	$6.20 \pm 0.06$	$5.38 \pm 0.06$	$4.96 \pm 0.06$	$5.05 \pm 0.06$	$4.99 \pm 0.06$	$4.71 \pm 0.06$	$4.63 \pm 0.06$
$\bar{\Lambda}\pi^-\pi^0$	$2.56 \pm 0.05$	$2.28 \pm 0.05$	$2.13 \pm 0.05$	$1.97 \pm 0.05$	$1.95 \pm 0.05$	$1.91 \pm 0.05$	$1.92 \pm 0.05$
$\bar{\Lambda}\pi^-\pi^+\pi^-$	$1.73 \pm 0.04$	$1.47 \pm 0.04$	$1.46 \pm 0.04$	$1.44 \pm 0.04$	$1.42 \pm 0.04$	$1.42 \pm 0.04$	$1.44 \pm 0.04$
$\bar{\Sigma}^0\pi^-$	$3.70 \pm 0.05$	$3.30 \pm 0.05$	$3.10 \pm 0.05$	$3.01 \pm 0.05$	$2.91 \pm 0.05$	$2.88 \pm 0.05$	$2.75 \pm 0.05$
$\bar{\Sigma}^-\pi^0$	$3.01 \pm 0.05$	$2.79 \pm 0.05$	$2.55 \pm 0.05$	$2.61 \pm 0.05$	$2.40 \pm 0.05$	$2.32 \pm 0.05$	$2.16 \pm 0.05$
$\bar{\Sigma}^-\pi^-\pi^+$	$3.23 \pm 0.05$	$2.97 \pm 0.05$	$2.84 \pm 0.05$	$2.72 \pm 0.05$	$2.65 \pm 0.05$	$2.51 \pm 0.05$	$2.40 \pm 0.05$

## 375 11 Summary

376 In summary, based on the 7 energy points samples collected at BESIII detector, the branching frac-  
 377 tions  $\Lambda_c^+ \rightarrow nK_S^0\pi^+\pi^0$  are measured for the first time, but is different from statistical isospin model  
 378 prediction. The table summarizes the results of branching fraction for this channel as Table 17.

Tab. 17: The branching fraction of  $\Lambda_c^+ \rightarrow nK_S^0\pi^+\pi^0$  process

Decay mode	Branching fraction( $\times 10^{-2}$ )
$\Lambda_c^+ \rightarrow pK^-\pi^+\pi^0$ (isospin measurement)	$4.46 \pm 0.30$ [4]
$\Lambda_c^+ \rightarrow nK^-\pi^+\pi^+$ (isospin measurement)	$1.87 \pm 0.12$ [5]
$\Lambda_c^+ \rightarrow pK_S^0\pi^+\pi^-$ (isospin measurement)	$1.60 \pm 0.12$ [4]
$\Lambda_c^+ \rightarrow nK_S^0\pi^+\pi^0$ (statistical isospin model prediction)	$1.54 \pm 0.08$ [24]
$\Lambda_c^+ \rightarrow nK_S^0\pi^+\pi^0$ (our measurement)	$0.85 \pm 0.13 \pm 0.03$

## 379 References

- 380 [1] G. S. Abrams *et al.* (Mark II Collaboration), Phys. Rev. Lett. 44, 10 (1980).
- 381 [2] P. A. Zyla *et al.* (Particle Data Group), [PTEP 2020, 083C01 \(2020\)](#) and 2021 update.
- 382 [3] [https://docbes3.ihep.ac.cn/DocDB/0010/001096/005/LamcNeutronX\\_draftv15.pdf](https://docbes3.ihep.ac.cn/DocDB/0010/001096/005/LamcNeutronX_draftv15.pdf)
- 383 [4] M. Ablikim *et al.* (BESIII Collaboration), Phys. Rev. Lett. **116**, no.5, 052001 (2016)  
384 doi:10.1103/PhysRevLett.116.052001 [arXiv:1511.08380 [hep-ex]].
- 385 [5] M. Ablikim *et al.* (BESIII Collaboration), Chin. Phys. C **47**, no.2, 023001 (2023) doi:10.1088/1674-  
386 1137/ac9d29 [arXiv:2210.03375 [hep-ex]].
- 387 [6] M. Ablikim *et al.* (BESIII Collaboration), Nucl. Instrum. Meth. A 614, 345 (2010).
- 388 [7] C. H. Yu *et al.*, Proceedings of IPAC2016, Busan, Korea, 2016, doi:10.18429/JACoW- IPAC2016-  
389 TUYA01.
- 390 [8] M. Ablikim *et al.* (BESIII Collaboration), Chin. Phys. C 44, 040001 (2020).
- 391 [9] X. Li et al., Radiat. Detect. Technol. Methods 1, 13 (2017); Y. X. Guo et al., Radiat. Detect. Technol.  
392 Methods 1, 15 (2017); P. Cao et al., Nucl. Instrum. Meth. A 953, 163053 (2020).
- 393 [10] S. Agostinelli *et al.* (Geant4 Collaboration), Nucl. Instrum. Meth. A 506, 250 (2003).
- 394 [11] S. Jadach, B. F. L. Ward and Z. Was, Comp. Phys. Commu. 130, 260 (2000); Phys. Rev. D 63,  
395 113009 (2001).
- 396 [12] D. J. Lange, Nucl. Instrum. Meth. A 462, 152 (2001); R. G. Ping, Chin. Phys. C 32, 599 (2008).
- 397 [13] J. C. Chen et al., Phys. Rev. D 62, 034003 (2000).
- 398 [14] [Official MC production for 4600-4700](#)
- 399 [15] R. M. Baltrusaitis *et al.* (MARK-III), Phys. Rev. Lett. **56**, 2140 (1986)  
400 doi:10.1103/PhysRevLett.56.2140
- 401 [16] G. Falldt (GF), Eur. Ph. J. A 52 141(2016); GF, A. Kupsc (AK), Phys. Lett. B 772 16(2017); GF,  
402 Phys. Rev. D 97 053002 (2018); GF, AK, S. Leupold, E. Perotti, arXiv:1809.04038 (2018).
- 403 [17] K. A. Olive *et al.* (Particle Data Group) Chin. Phys. C 38, 090001 (2014).

- 404 [18] M. Ablikim *et al.* (BESIII Collaboration), Phys. Rev. Lett. **118**, no.11, 112001 (2017)  
405 doi:10.1103/PhysRevLett.118.112001 [arXiv:1611.02797 [hep-ex]].
- 406 [19] <https://indico.ihep.ac.cn/event/8006/contributions/99144/attachments/52883/60932/Trk4180.pdf>
- 407 [20] [https://docbes3.ihep.ac.cn/DocDB/0006/000613/021/memo\\_v3.1.pdf](https://docbes3.ihep.ac.cn/DocDB/0006/000613/021/memo_v3.1.pdf)
- 408 [21] [https://docbes3.ihep.ac.cn/DocDB/0005/000520/001/KS\\_sys\\_v2.pdf](https://docbes3.ihep.ac.cn/DocDB/0005/000520/001/KS_sys_v2.pdf)
- 409 [22] [https://docbes3.ihep.ac.cn/DocDB/0004/000441/028/Lambda\\_c\\_nkspi\\_21Jan2016\\_2DFit.pdf](https://docbes3.ihep.ac.cn/DocDB/0004/000441/028/Lambda_c_nkspi_21Jan2016_2DFit.pdf)
- 410 [23] P. A. Zyla *et al.* (Particle Data Group), **PTEP** **2021**, 083C01 (2021).
- 411 [24] M. Gronau, J. L. Rosner and C. G. Wohl, Phys. Rev. D **97**, no.11, 116015 (2018)  
412 doi:10.1103/PhysRevD.97.116015 [arXiv:1808.03720 [hep-ph]].
- 413 [25] [https://docbes3.ihep.ac.cn/DocDB/0011/001123/001/note\\_nkspi\\_nksk\\_v0.8.pdf](https://docbes3.ihep.ac.cn/DocDB/0011/001123/001/note_nkspi_nksk_v0.8.pdf)

414 **A Appendices**

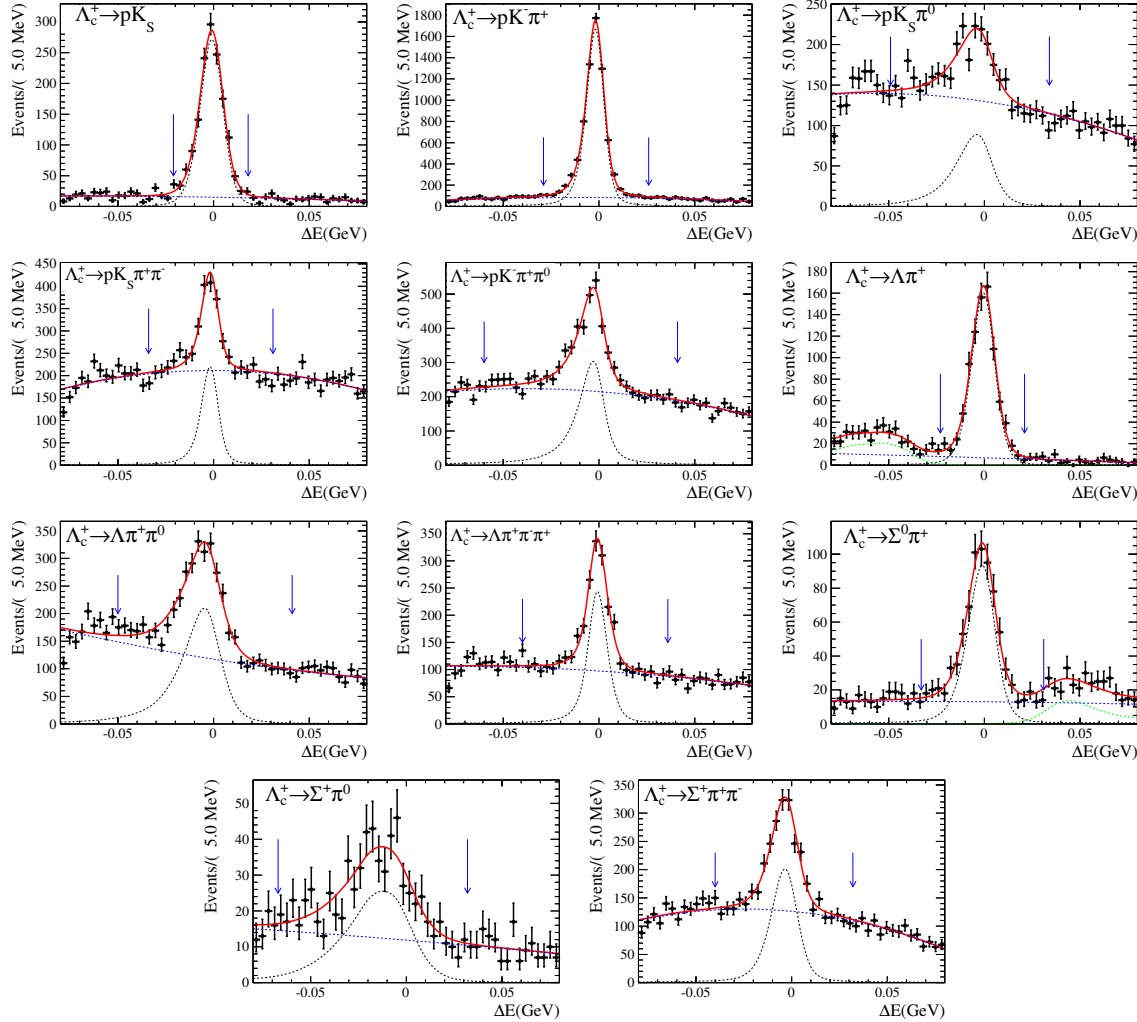


Fig. 17: Fit results of  $\Delta E$  distributions in data for different decay modes at  $\sqrt{s} = 4.600$  GeV. Points with error bars are data, red lines are the sum of fit functions, black dashed lines are signal shapes, blue dashed lines are the polynomial functions.

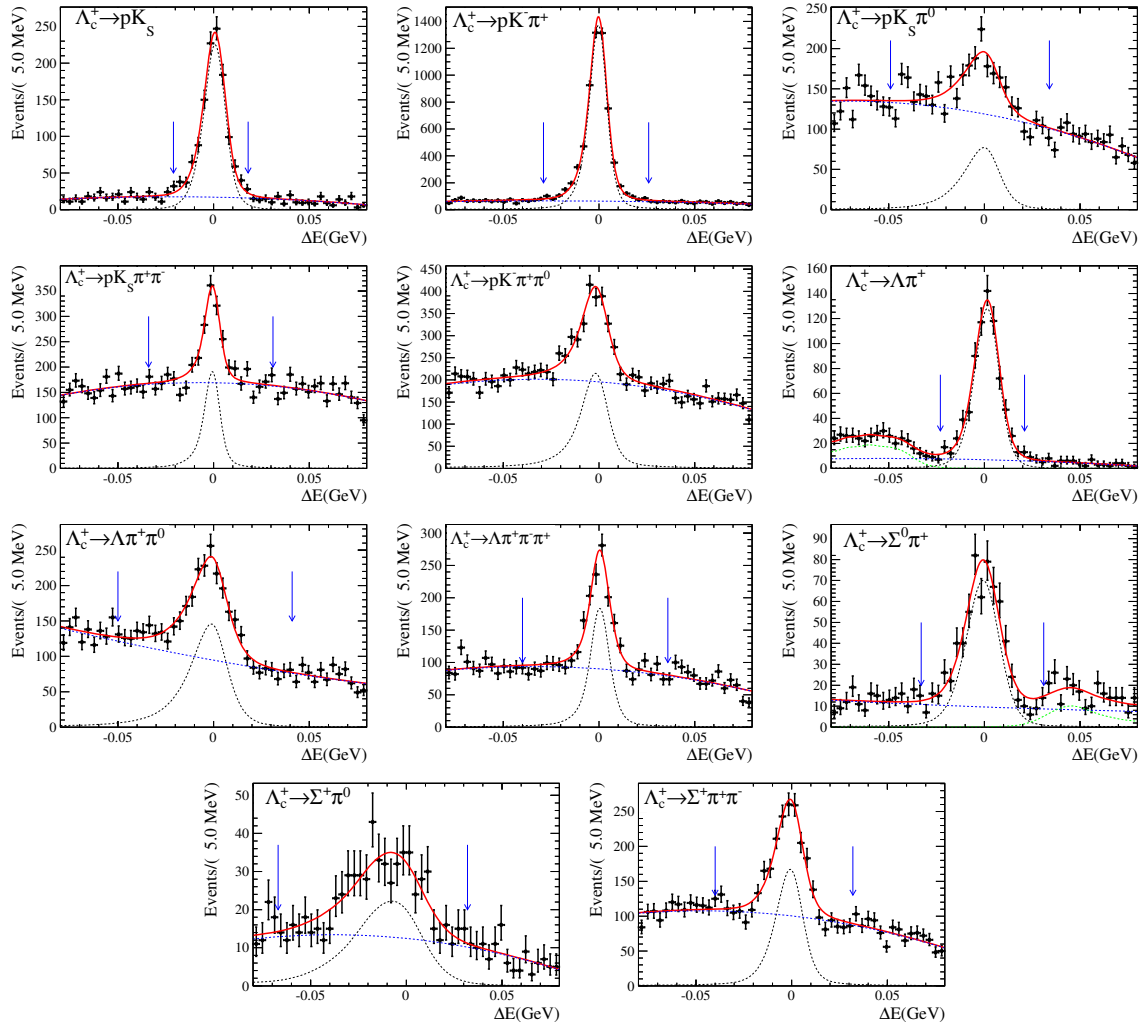


Fig. 18: Fit results of  $\Delta E$  distributions in data for different decay modes at  $\sqrt{s} = 4.628$  GeV. Points with error bars are data, red lines are the sum of fit functions, black dashed lines are signal shapes, blue dashed lines are the polynomial functions.

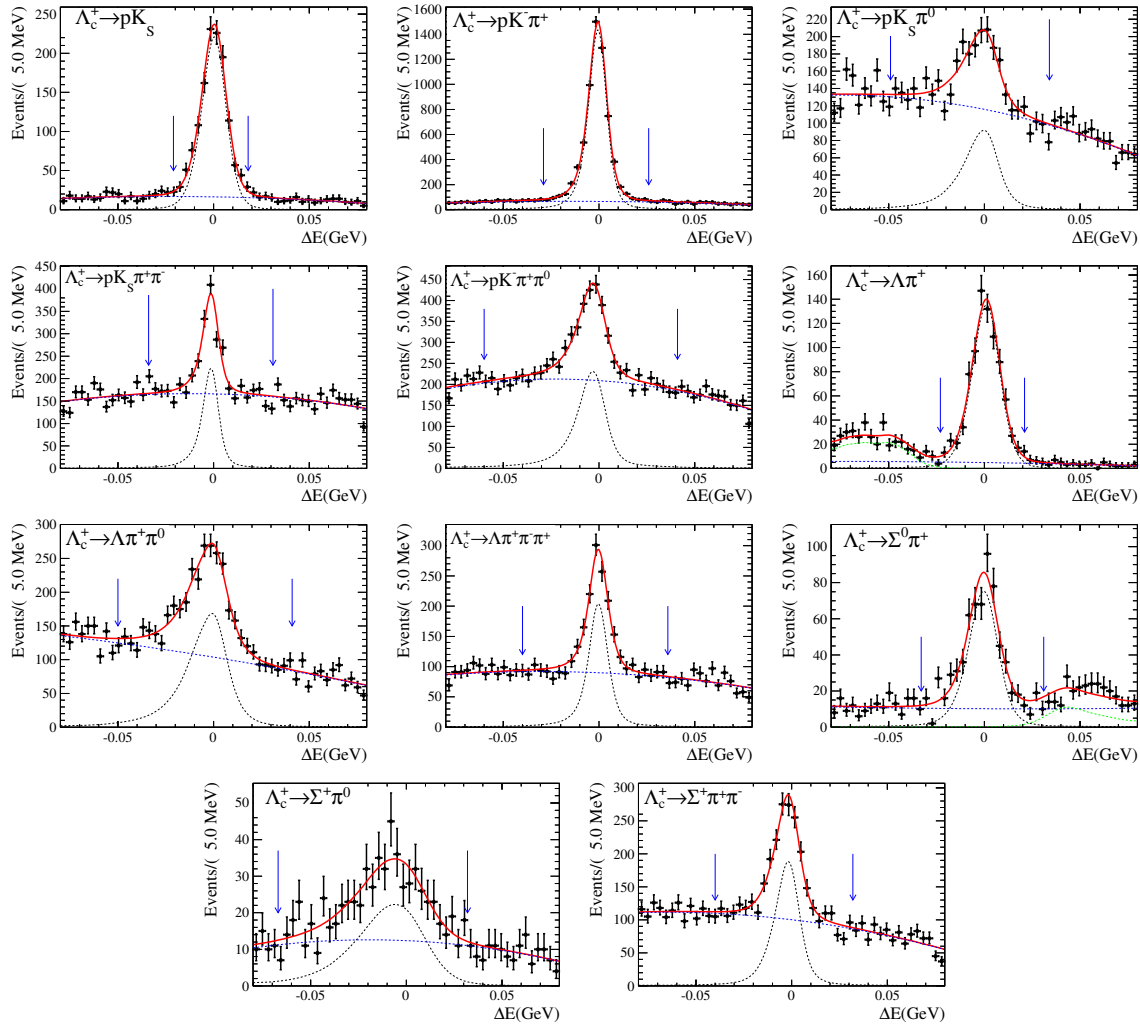


Fig. 19: Fit results of  $\Delta E$  distributions in data for different decay modes at  $\sqrt{s} = 4.641$  GeV. Points with error bars are data, red lines are the sum of fit functions, black dashed lines are signal shapes, blue dashed lines are the polynomial functions.

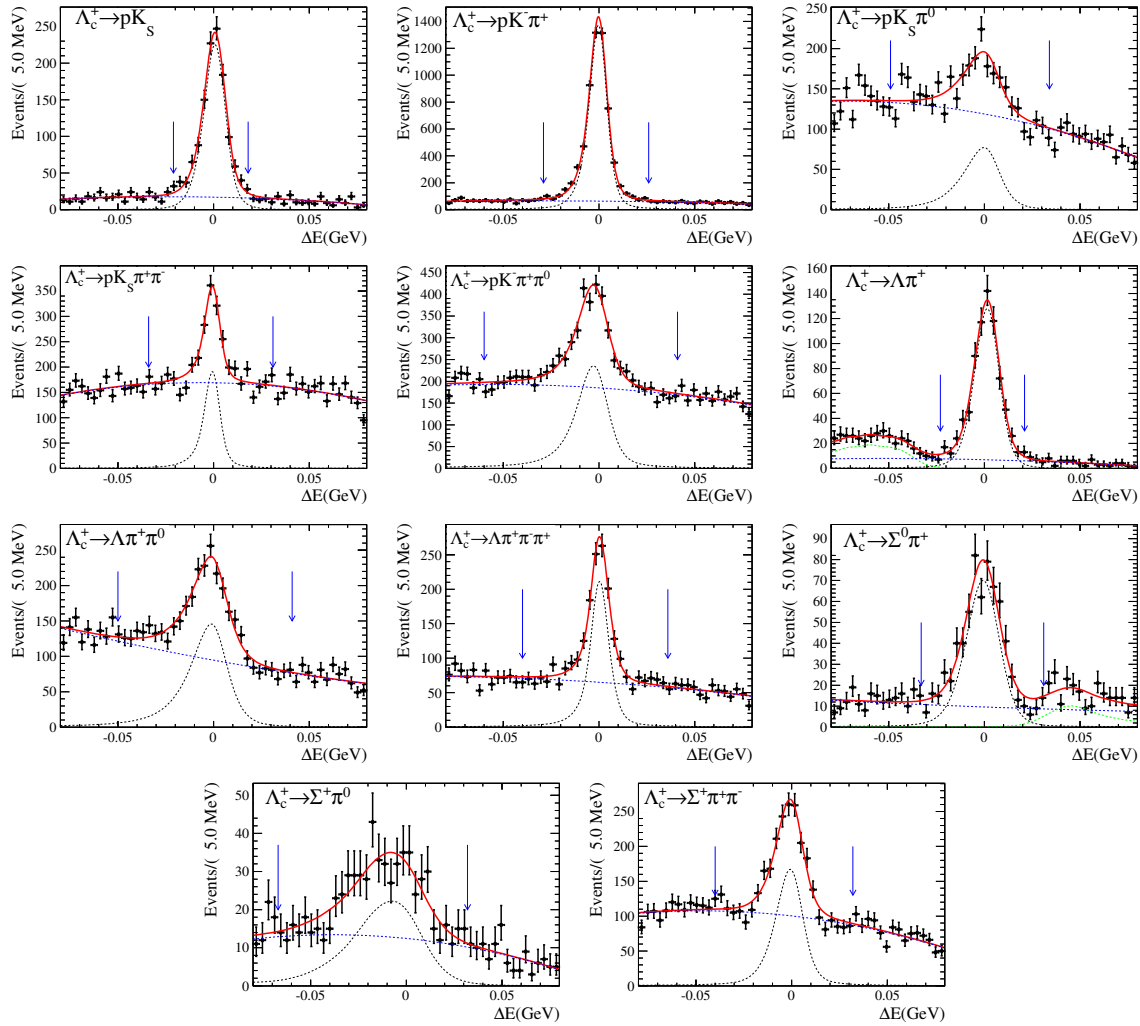


Fig. 20: Fit results of  $\Delta E$  distributions in data for different decay modes at  $\sqrt{s} = 4.661$  GeV. Points with error bars are data, red lines are the sum of fit functions, black dashed lines are signal shapes, blue dashed lines are the polynomial functions.

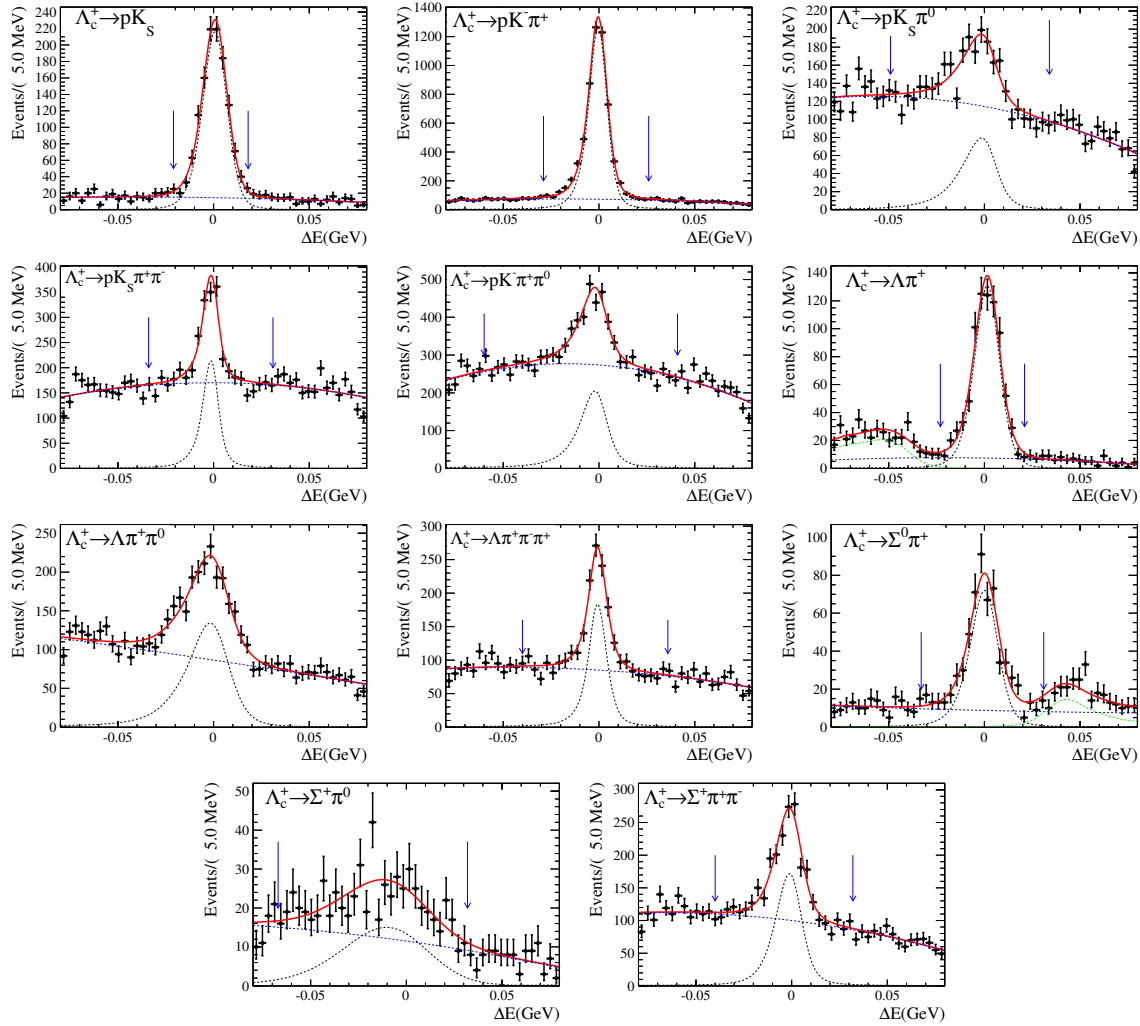


Fig. 21: Fit results of  $\Delta E$  distributions in data for different decay modes at  $\sqrt{s} = 4.682$  GeV. Points with error bars are data, red lines are the sum of fit functions, black dashed lines are signal shapes, blue dashed lines are the polynomial functions.

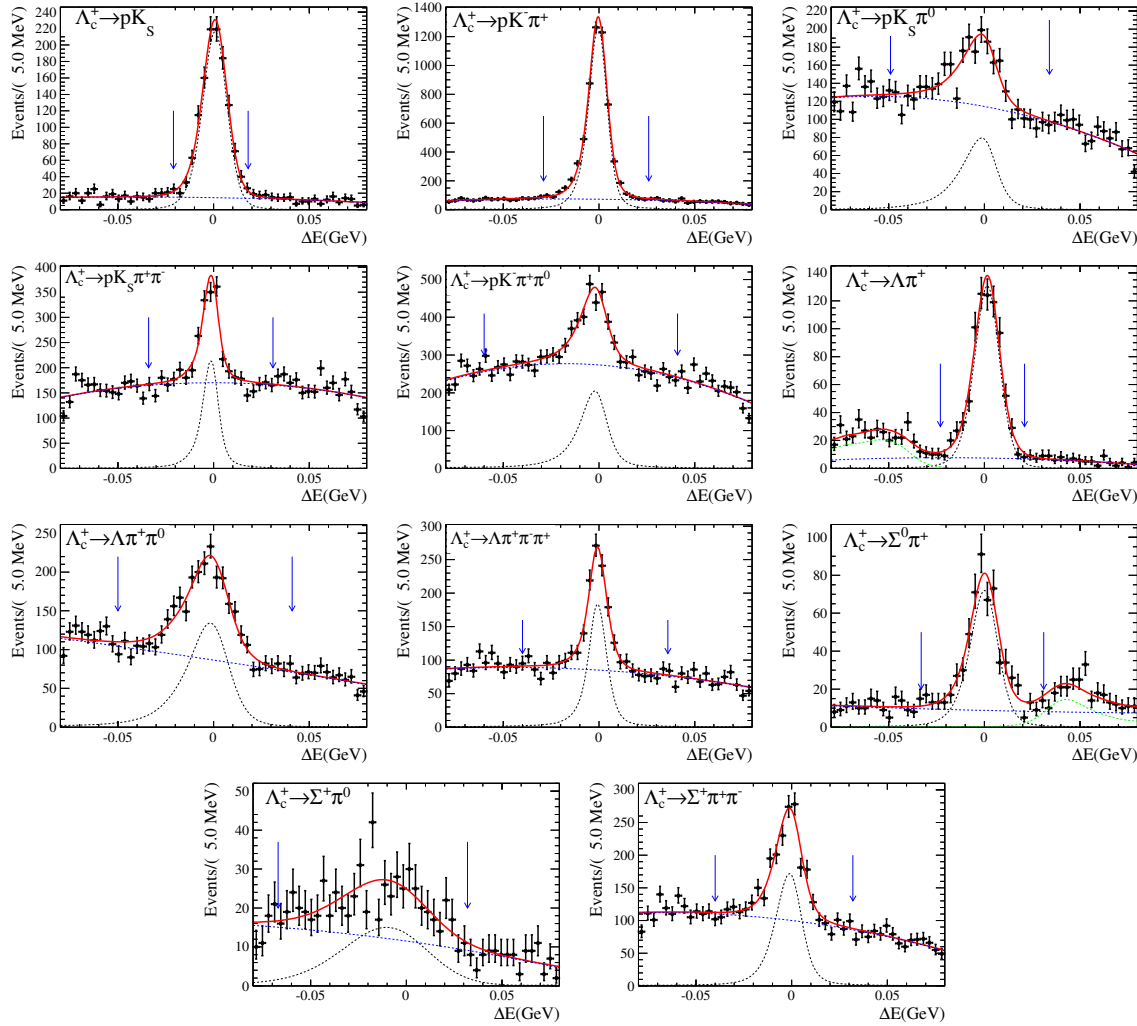


Fig. 22: Fit results of  $\Delta E$  distributions in data for different decay modes at  $\sqrt{s} = 4.699$  GeV. Points with error bars are data, red lines are the sum of fit functions, black dashed lines are signal shapes, blue dashed lines are the polynomial functions.

415 A.1 Other comparison with PHSP MC in the signal region

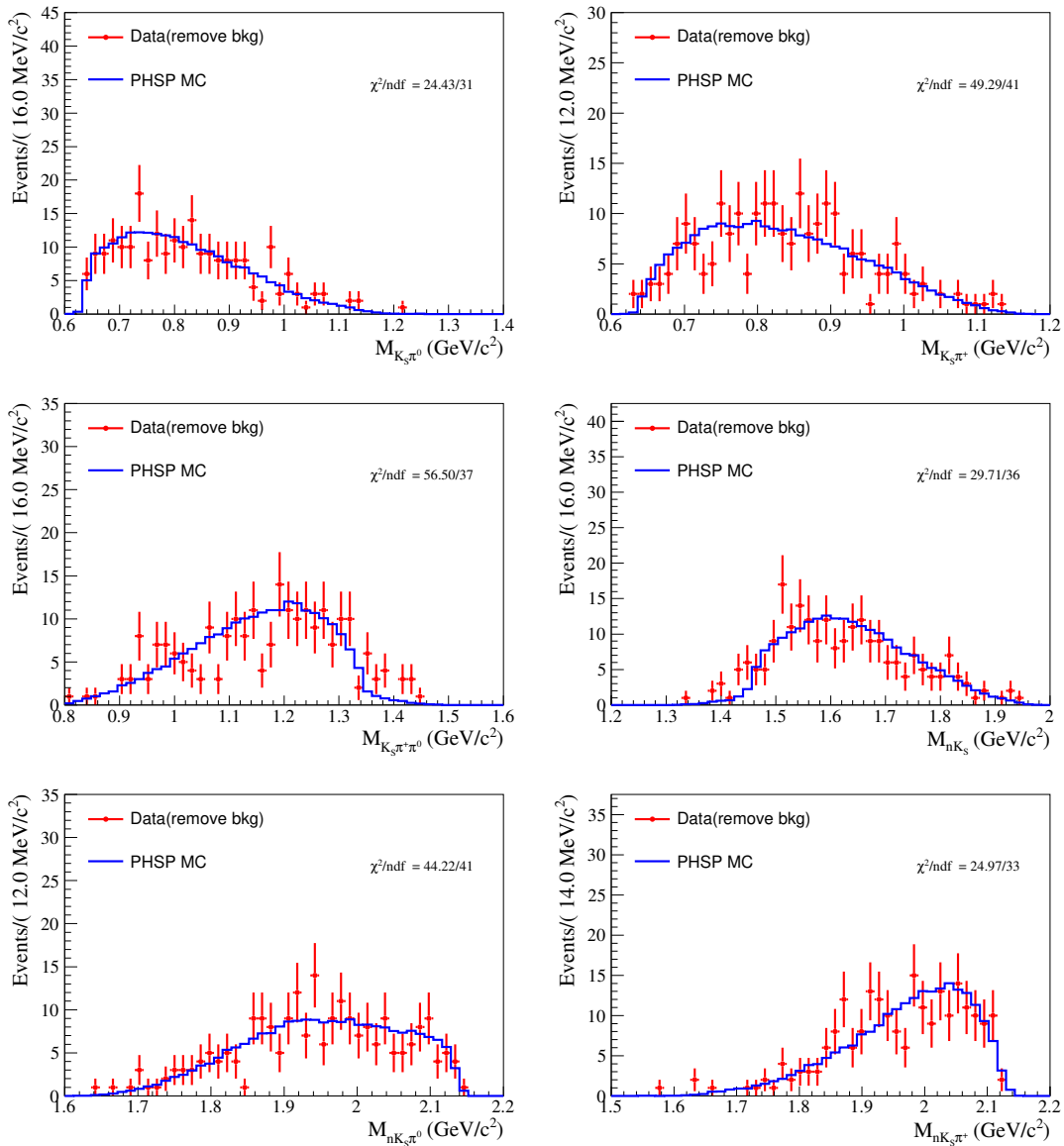


Fig. 23: The invariant mass distribution comparison in signal range.

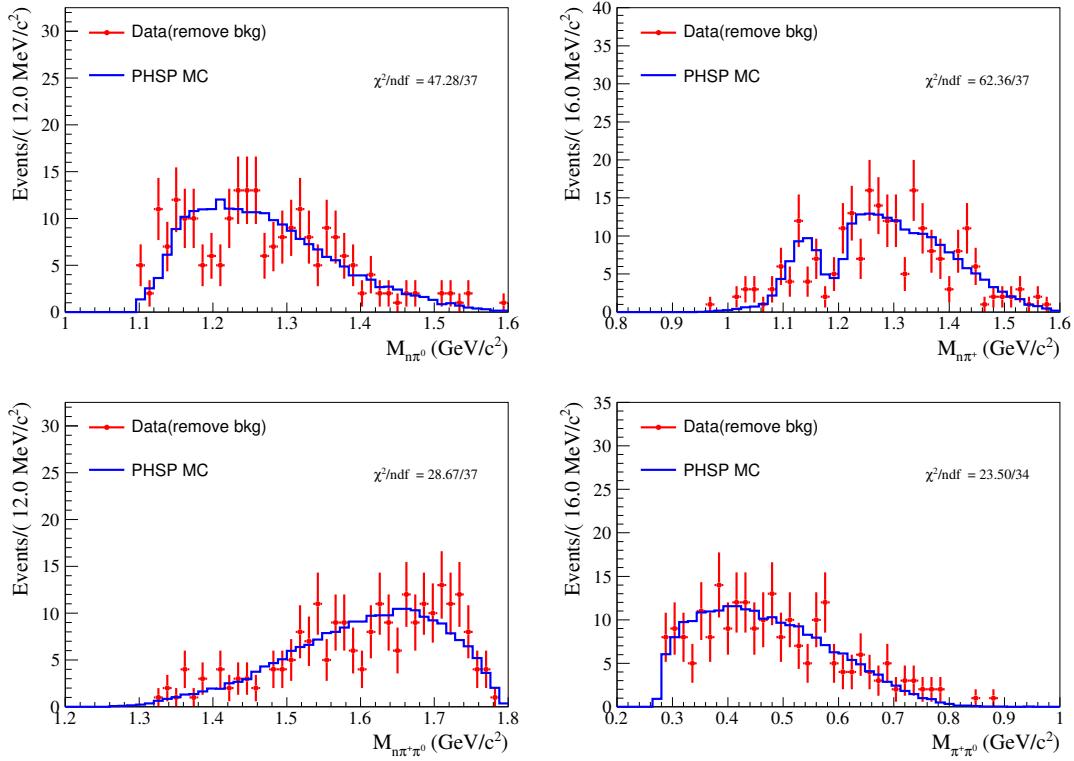


Fig. 24: The invariant mass distribution comparison in signal range.

416 A.2 Other comparison with Weight MC in the signal region

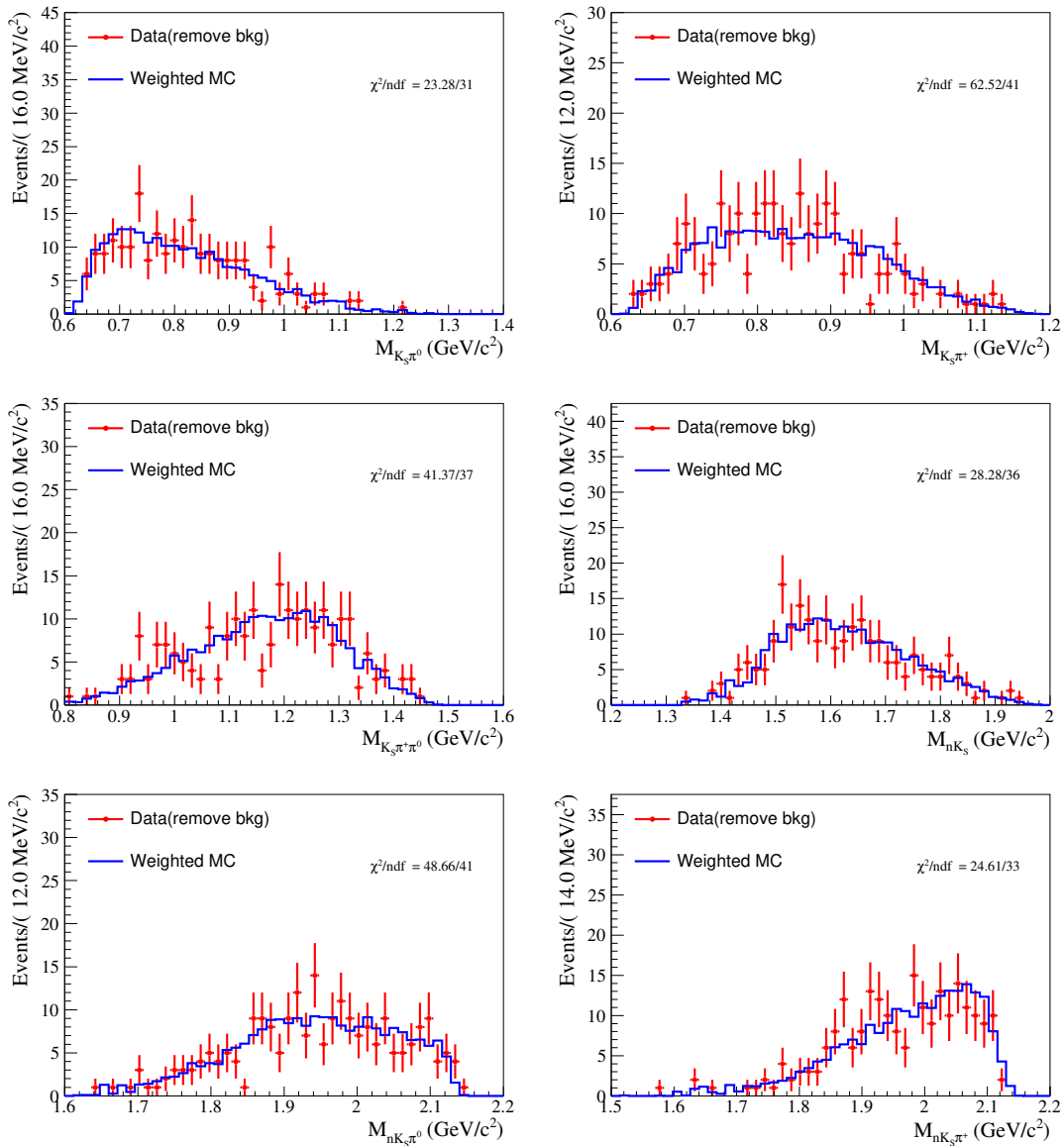


Fig. 25: The invariant mass distribution comparison in signal range.

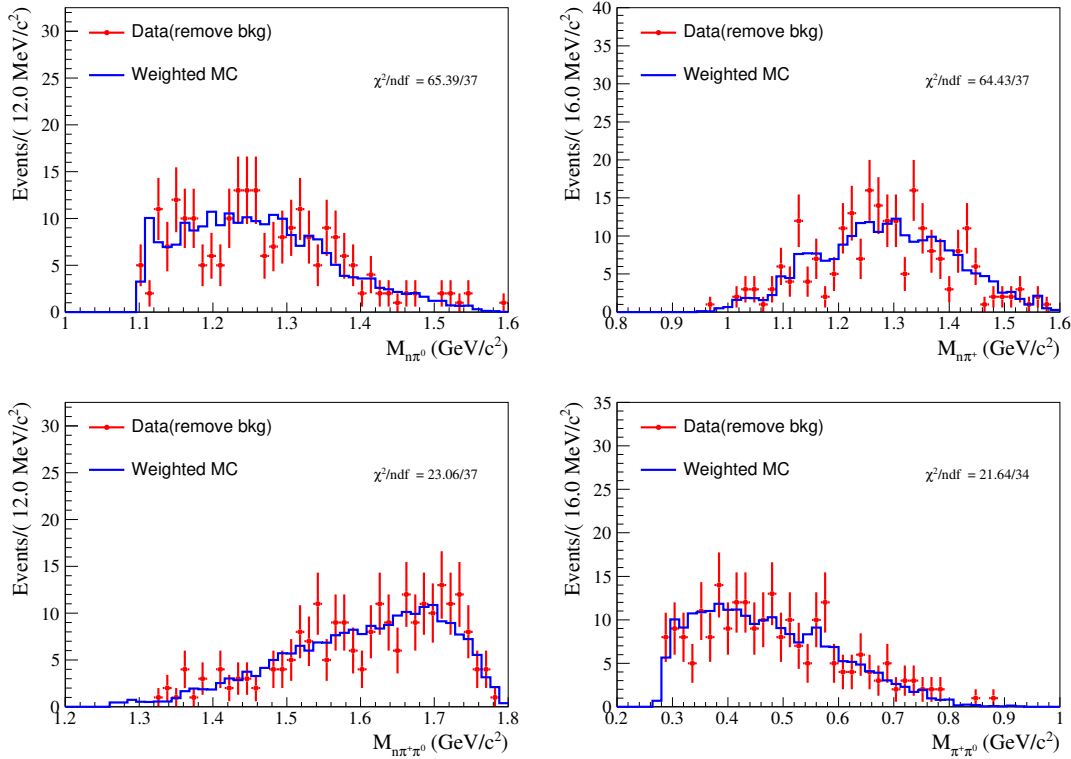


Fig. 26: The invariant mass distribution comparison in signal range.

<sup>417</sup> **A.3 Selection efficiency before vetoing peaking backgrounds**

Tab. 18: DT efficiencies(%) which combined charge conjugation modes from  $\sqrt{s} = 4.600$  GeV to 4.699 GeV.

modes	4.600 GeV	4.612 GeV	4.628 GeV	4.641 GeV	4.661 GeV	4.682 GeV	4.699 GeV
$\bar{p}K_S^0$	16.80	15.04	14.27	14.21	13.61	13.38	12.85
$\bar{p}K^+\pi^-$	16.17	14.58	14.20	14.06	13.70	13.35	12.81
$\bar{p}K_S^0\pi^0$	6.63	5.95	5.62	5.47	5.44	5.15	4.93
$\bar{p}K_S^0\pi^-\pi^+$	6.07	5.16	4.99	4.87	4.86	4.69	4.56
$\bar{p}K^+\pi^-\pi^0$	6.39	5.59	5.26	5.20	5.03	4.70	4.69
$\bar{\Lambda}\pi^-$	14.65	12.73	12.07	11.95	14.87	11.20	10.86
$\bar{\Lambda}\pi^-\pi^0$	6.15	5.25	5.08	4.89	4.70	4.58	4.44
$\bar{\Lambda}\pi^-\pi^+\pi^-$	4.28	3.60	3.52	3.50	3.41	3.37	3.34
$\bar{\Sigma}^0\pi^-$	8.76	7.85	7.45	7.07	6.94	6.65	6.48
$\bar{\Sigma}^-\pi^0$	7.06	6.51	6.06	6.12	5.59	5.37	5.16
$\bar{\Sigma}^-\pi^-\pi^+$	7.63	7.06	6.66	6.53	6.31	5.97	5.73

## 418 A.4 IO check for branching fraction

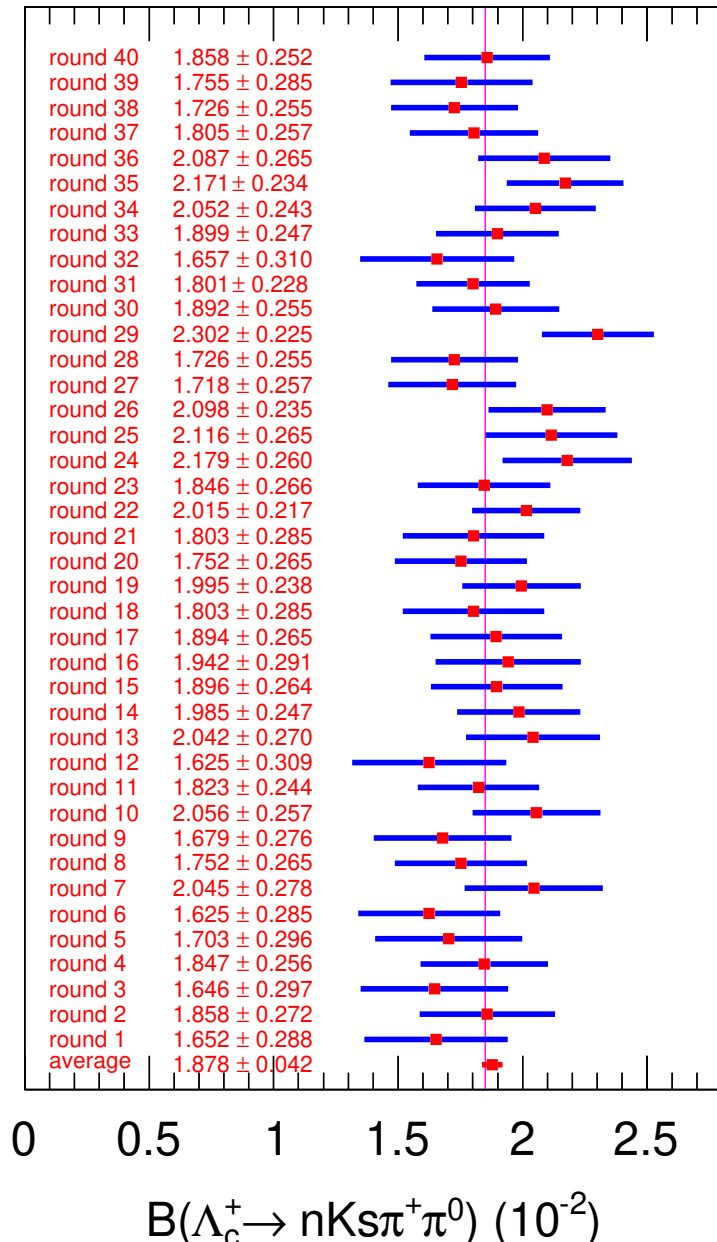


Fig. 27: The 40 times IO check for branching fraction.

419 **A.5 smearing parameters for the control sample  $\Lambda_c^+ \rightarrow \Lambda(n\pi^0)\pi^+$**

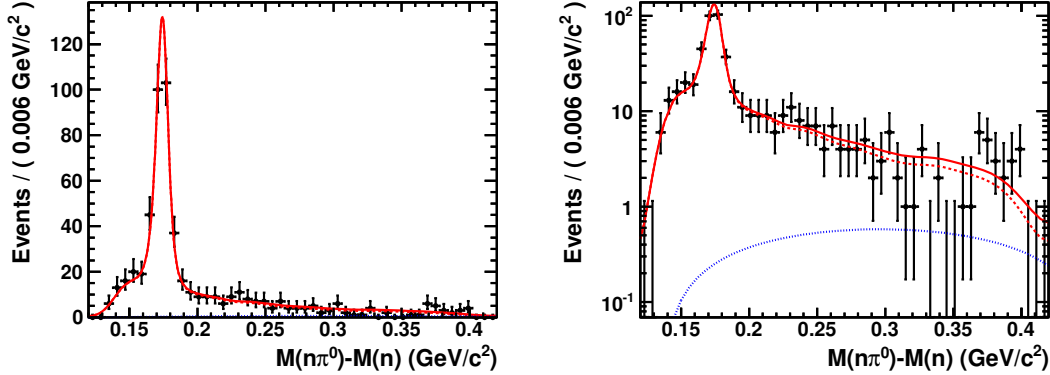


Fig. 28: The black dots with error bars are the data, the red solid line is the total fitting functions, the red dashed line is the signal function, the blue dotted line is the background function. The right figure shows log coordinates.

420 **A.6 Background analysis**

Tab. 19: Topology of  $\Lambda_c^+ \rightarrow nK_S^0\pi^+\pi^0$  in generic  $\Lambda_c^+$  inclusive MC sample.

rowNo	decay tree	decay final state	iDcyTr	nEtr	nCEtr
1	$\Lambda_c^+ \rightarrow \pi^0\pi^+\bar{K}^0n, \bar{K}^0 \rightarrow K_S^0, K_S^0 \rightarrow \pi^+\pi^-$	$\pi^0\pi^+\pi^+\pi^-n$	1	1863	1863
2	$\Lambda_c^+ \rightarrow \pi^+K^-p$	$\pi^+K^-p$	24	934	2797
3	$\Lambda_c^+ \rightarrow \pi^0\pi^+K^-p$	$\pi^0\pi^+K^-p$	6	352	3149
4	$\Lambda_c^+ \rightarrow \pi^0\pi^+\Lambda, \Lambda \rightarrow \pi^-p$	$\pi^0\pi^+\pi^-p$	55	232	3381
5	$\Lambda_c^+ \rightarrow \pi^+\pi^-\Sigma^+, \Sigma^+ \rightarrow \pi^0p$	$\pi^0\pi^+\pi^-p$	12	179	3560
6	$\Lambda_c^+ \rightarrow \bar{K}^0p, \bar{K}^0 \rightarrow K_S^0, K_S^0 \rightarrow \pi^+\pi^-$	$\pi^+\pi^-p$	0	163	3723
7	$\Lambda_c^+ \rightarrow \pi^0\bar{K}^0p, \bar{K}^0 \rightarrow K_S^0, K_S^0 \rightarrow \pi^+\pi^-$	$\pi^0\pi^+\pi^-p$	15	115	3838
8	$\Lambda_c^+ \rightarrow \pi^+\pi^-\bar{K}^0p, \bar{K}^0 \rightarrow K_S^0, K_S^0 \rightarrow \pi^+\pi^-$	$\pi^+\pi^+\pi^-\pi^-p$	34	105	3943
9	$\Lambda_c^+ \rightarrow \pi^+\pi^+\pi^-\Lambda, \Lambda \rightarrow \pi^-p$	$\pi^+\pi^+\pi^-\pi^-p$	19	96	4039
10	$\Lambda_c^+ \rightarrow \pi^+\Lambda, \Lambda \rightarrow \pi^-p$	$\pi^+\pi^-p$	118	93	4132
11	$\Lambda_c^+ \rightarrow K^{*+}\Lambda, K^{*+} \rightarrow \pi^+K^0, \Lambda \rightarrow \pi^0n, K^0 \rightarrow K_S^0, K_S^0 \rightarrow \pi^+\pi^-$	$\pi^0\pi^+\pi^+\pi^-n$	2	72	4204
12	$\Lambda_c^+ \rightarrow \pi^+\Sigma^0, \Sigma^0 \rightarrow \Lambda\gamma, \Lambda \rightarrow \pi^-p$	$\pi^+\pi^-p\gamma$	126	59	4263
13	$\Lambda_c^+ \rightarrow \pi^+\bar{K}^0n, \bar{K}^0 \rightarrow K_S^0, K_S^0 \rightarrow \pi^+\pi^-$	$\pi^+\pi^+\pi^-n$	31	57	4320
14	$\Lambda_c^+ \rightarrow \pi^0\pi^0\bar{K}^0p, \bar{K}^0 \rightarrow K_S^0, K_S^0 \rightarrow \pi^+\pi^-$	$\pi^0\pi^0\pi^+\pi^-p$	17	53	4373
15	$\Lambda_c^+ \rightarrow \pi^0\pi^+\pi^+\Sigma^-, \Sigma^- \rightarrow \pi^-n$	$\pi^0\pi^+\pi^+\pi^-n$	7	35	4408
16	$\Lambda_c^+ \rightarrow \pi^+\pi^+K^-n$	$\pi^+\pi^+K^-n$	8	31	4439
17	$\Lambda_c^+ \rightarrow \pi^0\pi^0\pi^+\Lambda, \Lambda \rightarrow \pi^-p$	$\pi^0\pi^0\pi^+\pi^-p$	11	26	4465
18	$\Lambda_c^+ \rightarrow \pi^0\Sigma^+, \Sigma^+ \rightarrow \pi^0p$	$\pi^0\pi^0p$	134	24	4489
19	$\Lambda_c^+ \rightarrow \pi^0\pi^+\Sigma^0, \Sigma^0 \rightarrow \Lambda\gamma, \Lambda \rightarrow \pi^-p$	$\pi^0\pi^+\pi^-\gamma$	23	23	4512
20	$\Lambda_c^+ \rightarrow \omega\Sigma^+, \omega \rightarrow \pi^0\pi^+\pi^-, \Sigma^+ \rightarrow \pi^+n$	$\pi^0\pi^+\pi^+\pi^-n$	4	21	4533
21	$\Lambda_c^+ \rightarrow K^{*+}\Sigma^{*0}, K^{*+} \rightarrow \pi^+K^0, \Sigma^{*0} \rightarrow \pi^0\Lambda, K^0 \rightarrow K_S^0, \Lambda \rightarrow \pi^0n, K_S^0 \rightarrow \pi^+\pi^-$	$\pi^0\pi^0\pi^+\pi^-n$	28	20	4553
22	$\Lambda_c^+ \rightarrow \pi^+\pi^-\bar{K}^0p, \bar{K}^0 \rightarrow K_L^0$	$K_L^0\pi^+\pi^-p$	22	19	4572
23	$\Lambda_c^+ \rightarrow \omega\Sigma^+, \omega \rightarrow \pi^0\pi^+\pi^-, \Sigma^+ \rightarrow \pi^0p$	$\pi^0\pi^0\pi^+\pi^-p$	30	19	4591

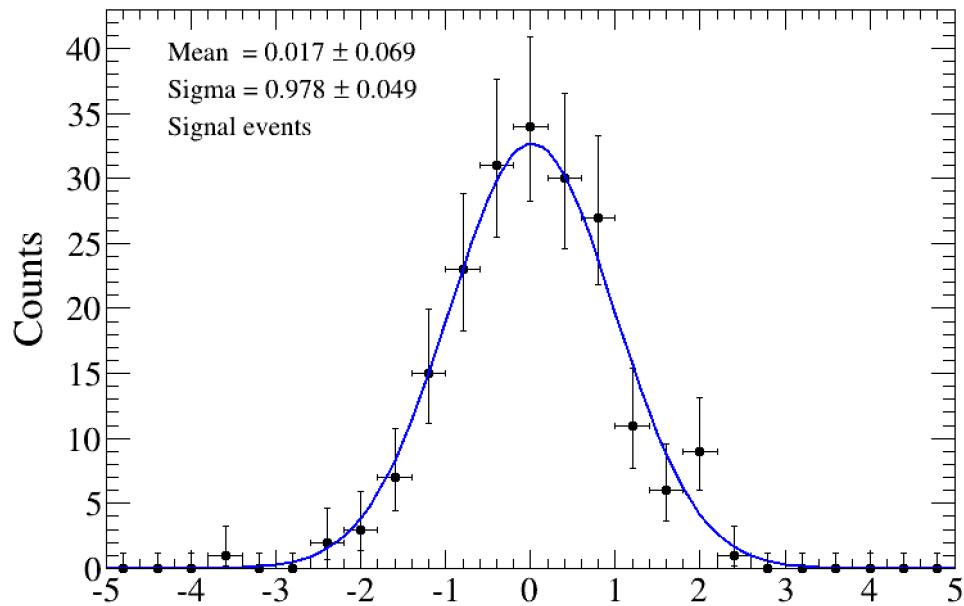
421 **B Check for fitting method**

Fig. 29: The pull distribution for 200 times IO check by performing two dimensional simultaneous fit.

422 **C Shape convolved by 2D Gaussian with correlation coefficients**

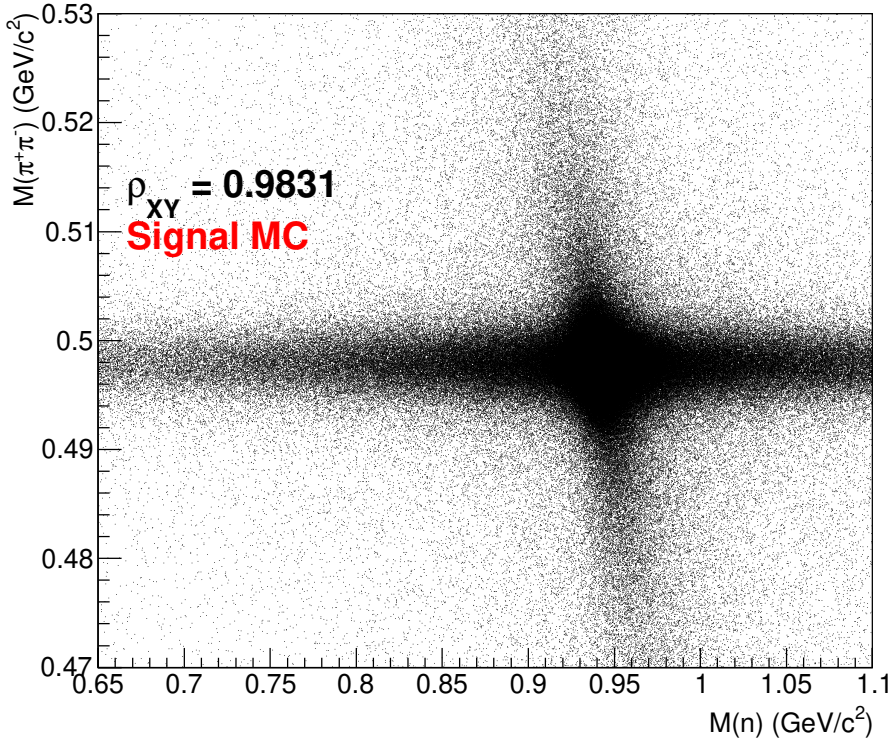


Fig. 30: The two dimensional  $M^2(n)$  and  $M_{\pi^+\pi^-}$  distribution from signal MC sample. The correlation coefficient  $\rho_{XY}$  is marked on the plot.

2 dimensional Gaussian function  $g(X_1, X_2)$  with no correlation can be expressed as,

$$g(X_1, X_2) = \frac{1}{2\pi\sigma_1\sigma_2} e^{-\frac{1}{2}(X-\mu)^T V^{-1}(X-\mu)} dX_1 dX_2, V^{-1} = \begin{bmatrix} \frac{1}{\sigma_1^2} & 0 \\ 0 & \frac{1}{\sigma_2^2} \end{bmatrix}.$$

Here, we consider a simple case where the mean value and standard deviation are 0 and 1, respectively, hence we have

$$g(X_1, X_2) = \frac{1}{2\pi} e^{-\frac{1}{2}X^T X} dX_1 dX_2.$$

We give  $X$  a linear transformation  $Y = AX + \mu$ , and the distribution  $g(X_1, X_2)$  becomes

$$\begin{aligned} g'(Y_1, Y_2) &= \frac{1}{2\pi|A|} e^{-\frac{1}{2}(Y-\mu)^T A^T A^{-1}(Y-\mu)} dY_1 dY_2 \\ &= \frac{1}{2\pi|A|} e^{-\frac{1}{2}(Y-\mu)^T V'^{-1}(Y-\mu)} dY_1 dY_2, \end{aligned}$$

where  $V'$  denotes  $AA^T$ . If  $Y$  obeys 2 dimensional Gaussian distribution with correlation, the expression of  $V'$  should be

$$V' = \begin{bmatrix} \sigma_1^2 & \rho\sigma_1\sigma_2 \\ \rho\sigma_1\sigma_2 & \sigma_2^2 \end{bmatrix}.$$

423 Hence the transformation matrix  $A$  is sufficed to satisfy  $V' = A^2$ .

424 **D 2D fit to the distributions of the invariant mass of  $n$  and  $\pi^+\pi^-$**

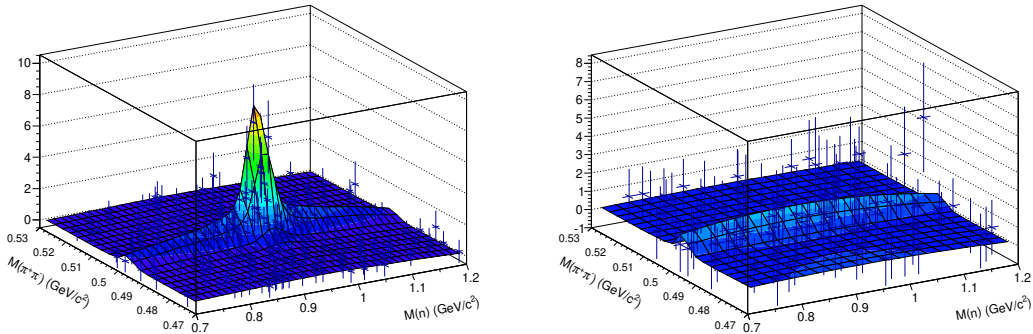


Fig. 31: 2D fit to the distributions of the invariant mass of  $n$  and  $\pi^+\pi^-$  in signal (left plot) and side-band (right plot) regions, respectively.